Generative Models: What Do They Know? Do They Know Things? Let's Find Out!

Anonymous authors
Paper under double-blind review

Abstract

Generative models excel at creating images that closely mimic real scenes, suggesting they inherently encode scene representations. We introduce Intrinsic LoRA (I-LoRA), a general approach that uses Low-Rank Adaptation (LoRA) to discover scene intrinsics such as normals, depth, albedo, and shading from a wide array of generative models. I-LoRA is lightweight, adding minimally to the model's parameters and requiring very small datasets for this knowledge discovery. Our approach, applicable to Diffusion models, GANs, and Autoregressive models alike, generates intrinsics using the same output head as the original images. We show a correlation between the generative model's quality and the extracted intrinsics' accuracy through control experiments. Finally, scene intrinsics obtained by our method with just hundreds to thousands of labeled images, perform on par with those from supervised methods trained on millions of labeled examples.

1 Introduction

Generative models can produce high-quality images almost indistinguishable from real-world photographs. They seem to demonstrate a profound understanding of the world, capturing nuances of realistic object placement, appearance, and lighting conditions. Yet, it remains an open question how these models encode such detailed knowledge, and whether representations of scene intrinsics exist in these models and can be extracted explicitly.

Why is this an important question? Understanding the basis of generative models' realistic outputs could enhance our grasp of the physical world through computational eyes, potentially refining image generation and interpretation processes across various applications. Our primary motivation is to explore whether intrinsic properties can be extracted from various generative models using the same approach. This lays the groundwork for future applications, such as improving the primary generation capabilities of these models. Developing a universally optimal method for this extraction has been the ultimate goal, yet it has eluded researchers in both computer vision and other fields, such as NLP, where this effort has been ongoing for years (e.g., Belinkov & Glass (2019); Ettinger (2020)). Our work aims to fill this gap, providing valuable insights into the inner workings of generative image models and their potential applications.

Recent work has begun to study this question. Bhattad et al. (2023a) demonstrated that StyleGAN can encode important scene intrinsics. Similarly, Zhan et al. (2023) showed that diffusion models can understand 3D scenes in terms of geometry and shadows. Chen et al. (2023) found that Stable Diffusion's internal activations encode depth and saliency maps that can be extracted with linear probes. Three independent efforts (Luo et al., 2023b; Tang et al., 2023; Hedlin et al., 2023) discovered correspondences in diffusion models. However, these insights often pertain to specific models, leaving a gap in our understanding of whether such encoding is ubiquitous across generative architectures. Our work addresses this gap by introducing a uniform approach, Intrinsic LoRA (I-LoRA) to extract intrinsic properties across multiple generative image model types, including GANs, Autoregressive, and Diffusion models.

Why study all types of generative models? Although diffusion models, such as Stable Diffusion (Rombach et al., 2022) and Imagen (Saharia et al., 2022), have garnered significant attention recently, the latest iterations of other model types like GigaGAN (Kang et al., 2023), CM3leon (Yu et al., 2023), and Parti (Yu et al., 2022)

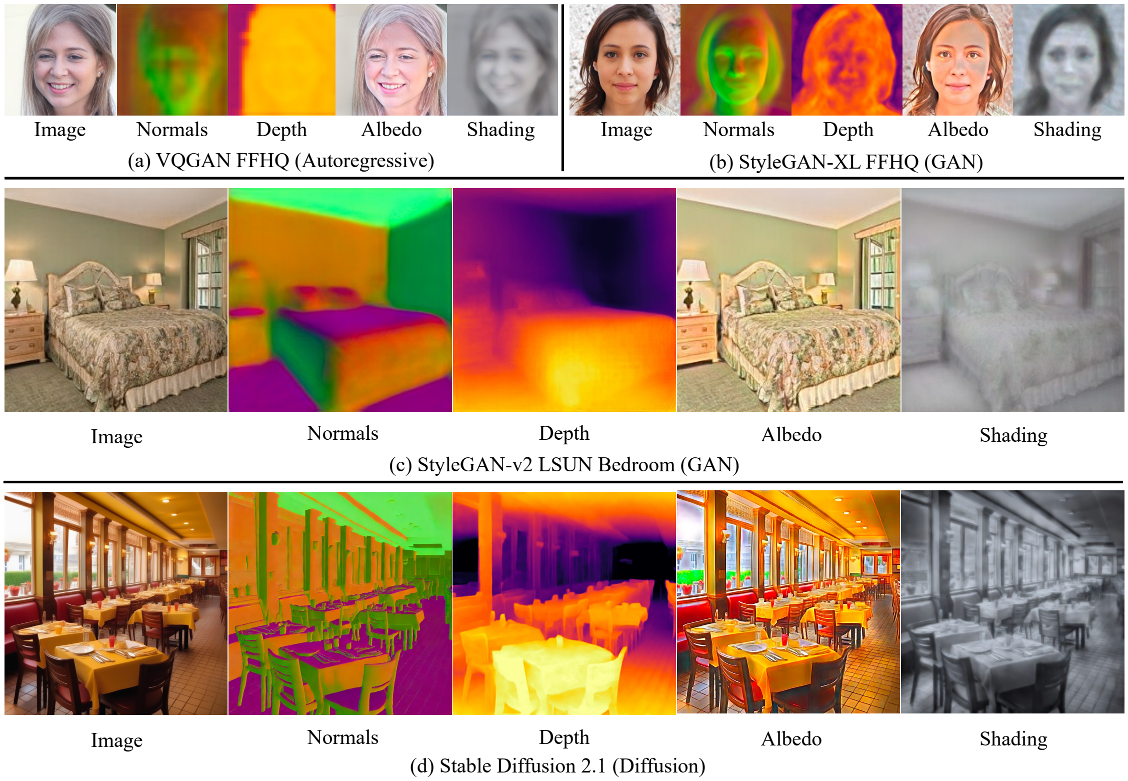
Image
Normals
Depth
Albedo
Shading
(a) VQGAN FFHQ (Autoregressive)
Image
Normals
Depth
Albedo
Shading
(b) StyleGAN-XL FFHQ (GAN)
Image
Normals
Depth
Albedo
Shading
(c) StyleGAN-v2 LSUN Bedroom (GAN)
Image
Normals
Depth
Albedo
Shading
(d) Stable Diffusion 2.1 (Diffusion)

Figure 1: We propose Intrinsic LoRA (I-LoRA), a model-agnostic, general approach for extracting visual knowledge from various generative models, including autoregressive, GANs, and diffusion models. Our method applies targeted, lightweight fine-tuning to modulate key feature maps, using low-rank adaptation (LoRA) on attention layers in VQGAN (a) and Stable Diffusion (d), and affine layers in StyleGAN (b and c). This allows us to discover fundamental scene intrinsics–normals, depth, albedo, and shading–directly from the models' learned representations, eliminating the need for additional task-specific decoding heads or layers.

have demonstrated a capacity to produce comparably high-quality images. Investigating these diverse models enables us to devise a general framework that applies not only to current models but is also adaptable to future developments and new generative models.

Our Contributions and Findings. We conduct our inquiry across a spectrum spanning diffusion, GANs, and autoregressive models to understand whether they encode fundamental scene intrinsics such as normals, depth, albedo, and shading (Barrow & Tenenbaum, 1978). We show that our method, I-LoRA, efficiently extracts these intrinsics across different model types with minimal computational overhead (less than 0.17% additional parameters for models like Stable Diffusion v1-5) and data requirements (as few as 250 labeled images). Importantly, I-LoRA does not require learning new heads, unlike Luo et al. (2023a) and Zhao et al. (2023), or complete fine-tuning (Zhao et al., 2023; Ke et al., 2023); instead, it predicts these intrinsic images from the same head or decoder that generates the images. This is significant because this simplified knowledge extraction reduces parameter requirements while maintaining efficiency and effectiveness.

A summary of our findings is presented in Tab. 1 and elaborated in Sec. 4. We observed significant improvement in the quality of recovered intrinsics when we used improved versions of Stable Diffusion (v1-1, v1-2, v1-5). In our control experiment, we found that randomly initialized Stable Diffusion architecture could not produce scene intrinsics. These findings suggest that the intrinsic knowledge within generative models is not accidental but a byproduct of large-scale learning to mimic image data. In summary, our contributions are:

- **Wide Applicability:** We validate I-LoRA 's capability to extract scene intrinsics (normals, depth, albedo and shading) across a broad spectrum of generative models, highlighting its adaptability to diverse architectures. We also show our method can be extended to non-generative models.

Table 1: Summary of scene intrinsics found across different generative models without changing generator head. ✓: Intrinsics can be extracted with high quality. ∼: Intrinsics cannot be extracted with high quality. ×: Intrinsics cannot be extracted.

Model	Pretrain Type	Domain	Normal	Depth	Albedo	Shading
VQGAN (Esser et al., 2020)	Autoregressive	FFHQ	∼	∼	✓	✓
SG-v2 (Karras et al., 2020b)	GAN	FFHQ	✓	∼	✓	✓
SG-v2 (Yu et al., 2021)	GAN	LSUN Bed	✓	✓	✓	✓
SG-XL (Sauer et al., 2022)	GAN	FFHQ	✓	∼	✓	✓
SG-XL (Sauer et al., 2022)	GAN	ImageNet	×	×	×	×
SD-UNet (single-step) (Rombach et al., 2022)	Diffusion	Open	✓	✓	✓	✓
SD (multi-step) (Rombach et al., 2022)	Diffusion	Open	✓	✓	✓	✓

- **Efficient and Lean Approach** to knowledge extraction: I-LoRA is highly efficient, requiring a little increase in parameters (less than 0.17% or as few as 0.04% for Stable Diffusion) and minimal training data, as few as 250 images.

- **Insights from Learned Priors:** Through control experiments with various Stable Diffusion configurations, we illustrate the role of learned priors in facilitating intrinsic representation, suggesting that the quality of intrinsics extracted is correlated to the visual quality of the generative model.

- **Competitive Quality of Intrinsics:** Our method, supervised with hundreds to thousands of labeled images, generates intrinsics on par with or even better than those produced by the leading supervised techniques requiring millions of labeled images. Moreover, our method outperforms linear probing and full finetuning of models in the limited data regime scenarios.

2 Related Work

Generative Models: Generative Adversarial Networks (GANs) (Goodfellow et al., 2014) have been widely used for generating realistic images. Variants like StyleGAN (Karras et al., 2019), StyleGAN2 (Karras et al., 2020b) and GigaGAN (Kang et al., 2023) have pushed the boundaries in terms of image quality and control. Some work has explored the interpretability of GANs (Bau et al., 2020; Bhattad et al., 2023a), but little is known about their ability to capture scene intrinsics.

Diffusion models, such as Denoising Score Matching (Vincent, 2011) and Noise-Contrastive Estimation (Gutmann & Hyvärinen, 2010), have been used for generative tasks and are perhaps the most popular at the moment (Karras et al., 2022; Ho et al., 2020; Rombach et al., 2022). These models have been shown to understand complex scene intrinsics like geometry and shadows (Zhan et al., 2023), but the generalizability of this understanding across different scene intrinsics is largely unexplored.

Autoregressive models like PixelRNN (Van Den Oord et al., 2016) and PixelCNN (Van den Oord et al., 2016) generate images pixel-by-pixel, offering fine-grained control but at the cost of computational efficiency. More recently, VQ-VAE-2 (Razavi et al., 2019) and VQGAN (Esser et al., 2020) have combined autoregressive models with vector quantization to achieve high-quality image synthesis. While these models are powerful, their ability to capture and represent scene intrinsics has not been thoroughly investigated.

Scene Intrinsics Extraction: Barrow & Tenenbaum (1978) highlighted several fundamental scene intrinsics including depth, albedo, shading, and surface normals. A large body of work has focused on extracting some related properties, like depth and normals from images (Eigen et al., 2014; Long et al., 2015; Eftekhar et al., 2021; Kar et al., 2022; Ranftl et al., 2021; Bhat et al., 2023) using labeled annotated data. Labeled annotations of albedo and shading are hard to find and as the recent review in Forsyth & Rock (2021) shows, methods involving little or no learning have remained competitive. However, these methods often rely on supervised learning and do not explore the capabilities of generative models in this context.

Many recent studies have used generative models as pre-trained feature extractors or scene prior learners. They use generated images to enhance downstream discriminative models, fine-tune the original generative model for a new task, learn new layers or decoders to produce desired scene intrinsics (Abdal et al., 2021; Jahanian et al., 2021; Zhang et al., 2021b; Li et al., 2021; Noguchi & Harada, 2020; Bao et al., 2022; Xu et al., 2023; Sariyildiz et al., 2023; Zhao et al., 2023; Ke et al., 2023). InstructCV (Gan et al., 2023) executes computer vision tasks via natural language instructions, abstracting task-specific design choices. However, it requires re-training of the entire diffusion model. In contrast, we show that many generative models capture intrinsic image knowledge implicitly and do not require specialized training to extract this information.

Knowledge in Generative Models: Several studies have explored the extent of StyleGAN's knowledge, particularly in the context of 3D information about faces (Pan et al., 2021; Zhang et al., 2021a). Yang et al. (2021) show GANs encode hierarchical semantic information across different layers. Further research has demonstrated that manipulating offsets in StyleGAN can lead to effective relighting of images (Bhattad et al., 2024; 2023b) and extraction of scene intrinsics (Bhattad et al., 2023a). Chen et al. (2023) found internal activations of the LDM encode linear representations of both depth data and a salient-object / background distinction. Wu et al. (2023) also demonstrate rich latent codes of diffusion models can be easily mapped to annotations with small amount of training samples. Recently, Tang et al. (2023); Luo et al. (2023b); Hedlin et al. (2023) found correspondence emerges in image diffusion models. Sarkar et al. (2023) showed generative models struggle to replicate accurate projective geometry in generated images.

Concurrent studies, such as the one by Luo et al. (2023a), have explored training task-specific "readout" networks to extract signals like pose, depth, and edges from feature maps in Stable Diffusion models for controlling image generation. Our goals are different: We are interested in recovering intrinsic images, while the aim of Luo et al. (2023a) is controlling image generation. Our method offers notable advantages in parameter efficiency: Our I-LoRA is approximately 5 times more parameter-efficient than readout networks in their application to SD v1-5 (compare 8.5M vs 1.59M). Lastly, the broad applicability of "readout" networks across various generative model types remains uncertain.

Another concurrent work Lee et al. (2023) applies a LoRA-like approach to adapt a pre-trained diffusion model for dense semantic tasks. Our work differs from theirs in several aspects: First, their goal is to use pre-trained diffusion models as strong priors for dense prediction. Second, their tasks are within restricted domains, such as bedrooms. Finally, they do not extend to the wide range of generative models our study explores. Our paper not only demonstrates I-LoRA's efficacy across different model architectures but also explores its application in a diverse array of scene contexts including real images.

Relation to Fine-Tuning and Linear Probing. Previous approaches for depth extraction from generative models fine-tune the entire model (Zhao et al., 2023; Ke et al., 2023) or apply linear probing (Chen et al., 2023). Fine-tuning alters the entire model with a specific dataset, transforming it into a new version that might lose its original image-generating capabilities. This raises questions about whether the depth perception was an inherent quality of the model or a result of the fine-tuning process. A drawback of linear probing lies in modeling each layer independently. While the tiny parameters, samples, and iterations required to train I-LoRA indicate that intrinsic information is easy to surface in generative models, the weak performance of linear probes indicates this knowledge is distributed throughout the network.

In contrast, I-LoRA performs efficient fine-tuning, and leverages the entire network's learned representation, modulating the internal flow of information for intrinsic extraction. This approach not only ensures a more holistic utilization of the network but also proves to be superior, as evidenced by our ablation studies. Another important property of I-LoRA is its preservation of the original's model output head to extract scene intrinsics—normals, depth, albedo, and shading as 3-channel, image-like maps, without requiring any new decoding layers. By doing so, it retains the original image generation functionality, while accessing the latent visual knowledge within generative models.

LoRA (Low-Rank Adaptation). LoRA (Hu et al., 2022), originally proposed to reduce the cost of fine-tuning large language models for downstream tasks, introduces trainable low-rank decomposed matrices into specific layers of the model architecture. These matrices are the only components updated during task-specific optimization. This results in a significant reduction in the number of trainable parameters, ensuring only slight modifications to the model, and preserving its core functionality and accessibility.

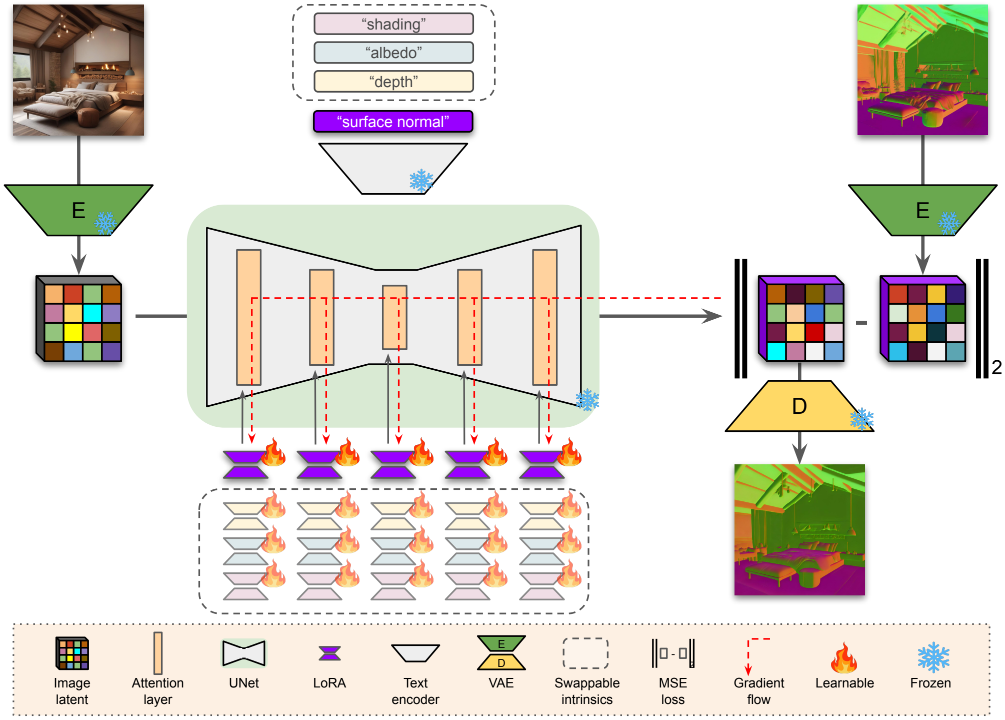

Figure 2: Overview of I-LoRA applied to Stable Diffusion's UNet in a single-step manner. We adopt an efficient fine-tuning approach, specifically low-rank matrices corresponding to key feature maps – attention matrices – to reveal scene intrinsics. Distinct low-rank adaptors (LoRA) are optimized for each intrinsic (***violet*** adaptors for surface normals; swappable with other intrinsics). We use a few labeled examples for this fine-tuning and directly extract scene intrinsics using the same decoder that generates images, circumventing the need for specialized decoders or comprehensive model re-training.

3 Intrinsic LoRA

A generative model G maps noise/conditioning information z to an RGB image $G(z) \in \mathbb{R}^{H\times W\times 3}$. We seek to augment G with a small set of parameters θ that allow us to produce, using the same architecture as G, an image-like map with up to three channels, representing scene intrinsics like surface normals.

I-LoRA's Learning Framework. Our method, Intrinsic LoRA(I-LoRA), learns to extract intrinsic properties of an image (such as depth) using a small number of labeled examples (image/depth map pairs) as supervision. In cases where we do not have access to the actual intrinsic properties, we use models trained on large datasets to generate estimated intrinsics (such as estimated depth for an image) as pseudo-ground truth, used as training targets for G_θ. To optimize θ of G_θ using a pseudo-ground truth predictor Φ, we minimize the objective:

$$\min_\theta \mathbb{E}_z[d(G_\theta(z), \Phi(G(z)))], \tag{1}$$

where d is a distance metric that depends on the intrinsics we wish to learn.

Diffusion models require special treatment since they are effectively image-to-image and not noise-to-image. During inference, diffusion models repeatedly receive a noisy image as input. Thus instead of conditioning noise z we feed an image x(generated or real) to a diffusion model G. In this case, given a real image x, our objective function becomes $\min_\theta \mathbb{E}_x[d(G_\theta(x), \Phi(x))]$.

For surface normals Φ is Omnidatav2-Normal (Eftekhar et al., 2021; Kar et al., 2022). To generate pseudo ground truth for depth we use ZoeDepth (Bhat et al., 2023) as the predictor Φ. For Albedo and Shading Φ is Paradigms (Forsyth & Rock, 2021; Bhattad & Forsyth, 2022). For SG2, SGXL and VQGAN, d in Eq.1 is

$$d(x, y) = 1 - cos(x, y) + \|x - y\|_1 \tag{2}$$

for normal and MSE for other intrinsics. For latent diffusion, there isn't a clear physical meaning to the relative angle of latent vectors in encoded normals, so we use the standard objective of MSE for all intrinsics.

We use LoRA, a parameter-efficient adaptation technique, to recover image intrinsics from generative models. LoRA introduces a low-rank weight matrix W^*, which has a lower rank than the original weight matrix $W \in \mathbb{R}^{d_1 \times d_2}$. This is achieved by factorizing W^* into two smaller matrices $W_u^* \in \mathbb{R}^{d_1 \times d^*}$ and $W_l^* \in \mathbb{R}^{d^* \times d_2}$, where d^* is chosen such that $d^* \ll \min(d_1, d_2)$. The output o for an input activation a is then given by:

$$o = Wa + W^*a = Wa + W_u^* W_l^* a. \tag{3}$$

To preserve the original model's behavior at initialization, W_u^* is initialized to zero. We next describe how we leverage LoRA modules to extract intrinsics from Diffusion models, GANs, and Autoregressive models.

Applying I-LoRA. For **diffusion models**, I-LoRA adaptors are learned atop cross-attention and self-attention layers. The UNet is utilized as a dense predictor, transforming an RGB input into intrinsics in one step. This approach, favoring simplicity and effectiveness, delivers superior quantitative results. Depending on the intrinsic of interest, the textual input varies among "surface normal", "depth", "albedo", or "shading". Fig. 2 illustrates the I-LoRA pipeline. For **GANs**, I-LoRA modules are integrated with the affine layers that map from w-space to s-space (Wu et al., 2021). In the case of **VQGAN, an autoregressive model**, I-LoRA is applied to the convolutional attention layers within the decoder.

4 Experiments

In this section, we outline I-LoRA's contributions, demonstrating its general applicability across generative models (Sec. 4.1) and its efficiency in terms of parameters and labeling (Sec. 4.2). Control experiments provide evidence of I-LoRA's effectiveness (Sec. 4.3), while comparative analysis establish its superiority over both fine-tuning and linear probing methods (Sec. 4.4). Additional ablation studies and baseline comparisons further confirm I-LoRA's robustness (Appendix B). Note: our analysis in Sec. 4.2 uses a single-step I-LoRA model for intrinsic image extraction from stable diffusion. In Sec. 5, we discuss the challenge of naively applying I-LoRA to a multi-step Stable Diffusion model. To address this, we propose a simple modification to the architecture by adding an extra, non-learned layer for improved intrinsic image extraction. We refer to this modified model as **Augmented I-LoRA** (I-LoRA$_{\text{AUG}}$).

4.1 I-LoRA is General and Universally Applicable

We evaluate I-LoRA across diverse generative models, including StyleGAN-v2 (Yu & Smith, 2019), StyleGAN-XL (Sauer et al., 2022), and VQGAN (Esser et al., 2020), trained on datasets like FFHQ (Karras et al., 2020b), LSUN Bedrooms (Yu et al., 2015), and ImageNet (Deng et al., 2009). I-LoRA adaptors are tailored to each model and dataset to extract intrinsics: surface normals, depth, albedo, and shading, demonstrating broad applicability and robustness in both qualitative assessments (Fig. 1, 3, 4, 6) and quantitative (Tab. 2 on generated images, Tab. 3 on real images). In all experiments – covering both generated and real images – we use pseudo-ground truth from pre-trained models as a supervisory signal for fine-tuning I-LoRA to discover scene intrinsics within generative models as previously mentioned in Sec. 3. We use I-LoRA with Rank 8 as default for all generative models if not otherwise mentioned.

We find I-LoRA can unearth intrinsic knowledge across almost all models tested, the notable exception is StyleGAN-XL trained on ImageNet. Where it yields qualitatively poor results, which we attribute to the model's limited ability to generate realistic images (Fig. 5). This suggests the quality of intrinsic extraction is correlated with the generative model's fidelity (see Sec. 4.3). In evaluations of generated images, our method is benchmarked against pseudo-ground truths derived from existing models, compensating for the lack of true ground truths. The performance of I-LoRA , gauged through these comparisons, provides useful indicators but must be interpreted within the context of the selected pseudo-ground truths.

Thanks to their architecture as image-to-image translators, diffusion models excel as powerful image generators. This feature simplifies their application to real images. Taking advantage of this, we apply I-LoRA to directly extract intrinsic images from Stable Diffusion's UNet in a single step. This method bypasses the

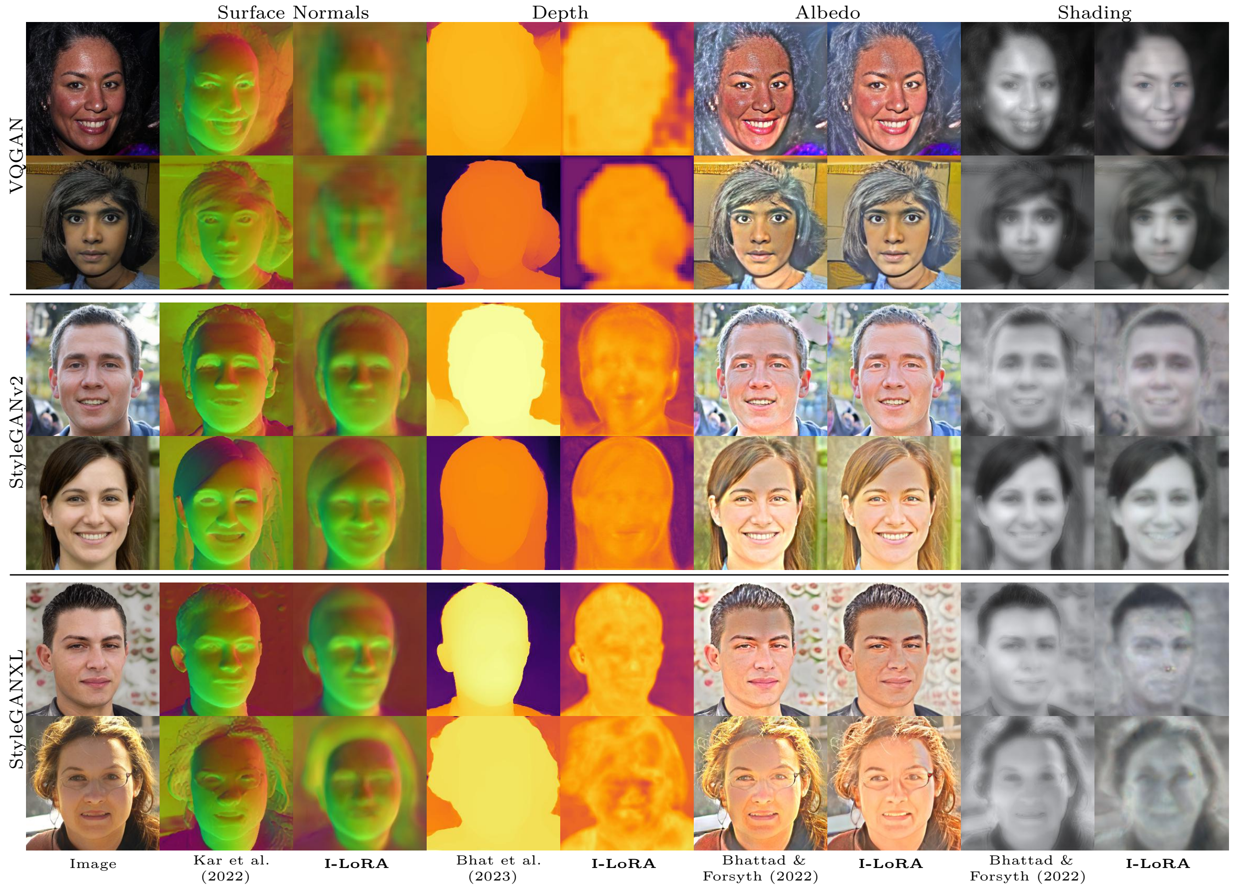

Figure 3: Scene intrinsics from different generators – VQGAN, StyleGAN-v2, and StyleGAN-XL – trained on FFHQ dataset: The "image" column shows the synthetic images produced by each model. Subsequent columns show four scene intrinsics extracted by a SOTA non-generative model and I-LoRA (ours).

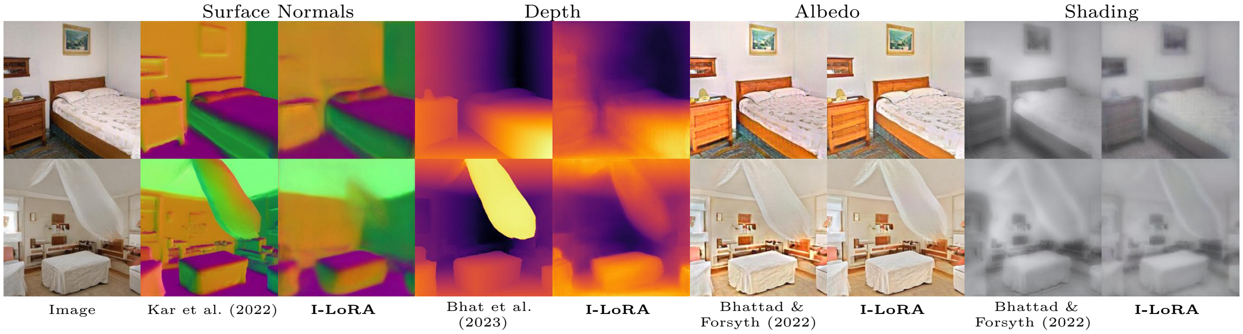

Figure 4: I-LoRA's extracted scene intrinsics from StyleGAN-v2 trained on LSUN bedroom images are competitive with task-specific models.

iterative reverse denoising process. The model receives a real image as input and outputs the corresponding image intrinsics through I-LoRA. Such direct application allows for evaluation against actual ground truth. This provides a definitive benchmark for assessing I-LoRA's effectiveness on DIODE dataset (Vasiljevic et al., 2019). We use the official training/evaluation split in all of our DIODE experiments. For training with fewer samples, we randomly chose samples from the official training partition. All the metrics we reported on DIODE are computed over the entire evaluation set. In Tab. 3, we find that I-LoRA not only matches but, in several metrics (median error for surface normals, RMSE for depth), surpasses the performance of Omnidata and ZoeDepth – the source of its training signal – while using significantly less data, parameters, and training time (see Sec.4.2).

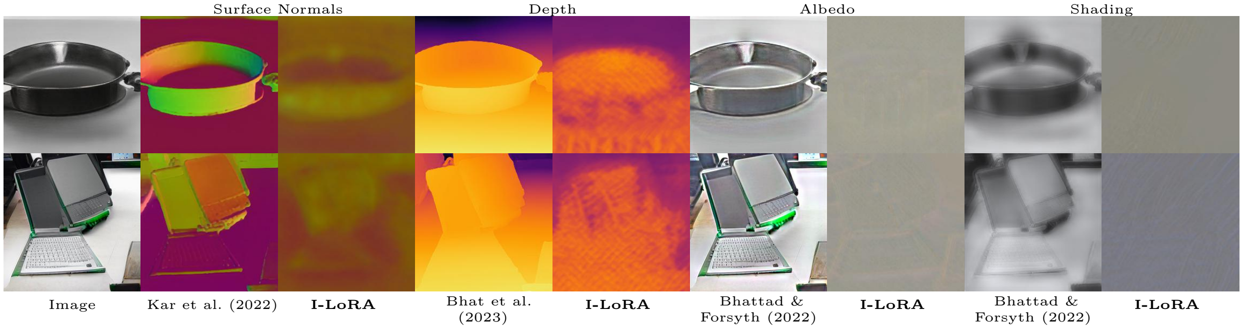

Figure 5: StyleGAN-XL trained on ImageNet. Top: pan, bottom: laptop, with the corresponding scene intrinsics (pseudo ground truth and extracted) alongside. The surface normals and depth maps, while capturing the basic shape and volume, lack precise detail and exhibit artifacts. Albedo and Shading extractions fail. These difficulties are correlated with the overall worse realism and consistency of the generated images.

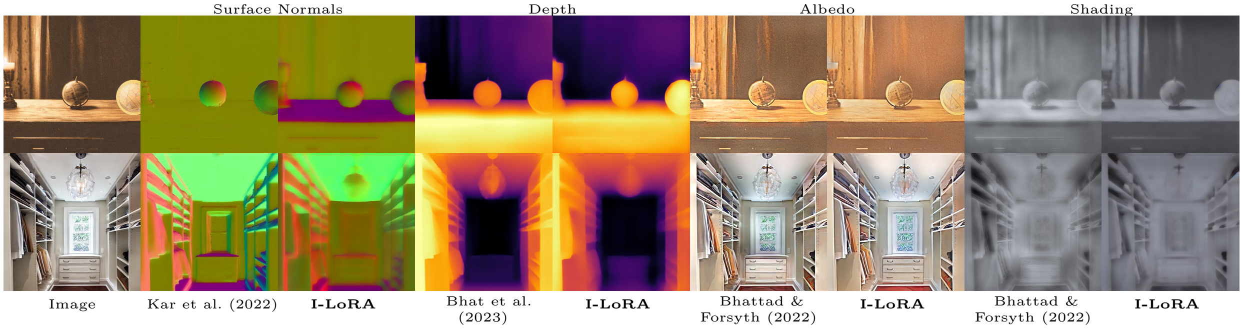

Figure 6: Scene intrinsics from I-LoRA applied to randomly generated images. I-LoRA accurately predicts the table's normal in the first row when compared to Kar et al. (2022). The globe in the right corner also appears to be closer to the camera in our depth compared to Bhat et al. (2023). In the second row, ceiling lamp normals are also visible in I-LoRA but not in Kar et al. (2022). The comparison highlights I-LoRA's ability to closely align with, and sometimes surpass, these supervised SOTA monocular predictors.

Table 2: Quantiative analysis of scene intrinsics extraction performance by I-LoRA on generated images. We compare with pseudo ground truths from Omnidata-v2 for surface normals, ZoeDepth for depth, and Paradigms for albedo and shading. Metrics include mean angular error, median angular error, and L1 error for surface normals; RMS and $\delta < 1.25$ for depth; RMS for albedo and shading.

Model	Pre-training Type	Domain	LoRA Param.	Surface Normal			Depth		Albedo	Shading
				Mean Error°↓	Median Error°↓	L1 Error$_{\times\ 100}$ ↓	RMS ↓	$\delta < 1.25_{\times 100\%}$ ↑	RMS ↓	RMS ↓
VQGAN	Autoregressive	FFHQ	0.18%	19.97	20.97	16.33	0.1819	62.33	0.0345	0.0106
StyleGAN-v2	GAN	FFHQ	0.57%	16.93	19.60	13.87	0.1530	90.74	0.0283	0.0110
StyleGAN-XL	GAN	FFHQ	0.29%	15.28	18.07	12.63	0.1337	93.87	0.0287	0.0125
StyleGAN-v2	GAN	LSUN Bedroom	0.57%	13.94	24.76	11.49	0.0897	66.88	0.0270	0.0074
StyleGAN-XL	GAN	ImageNet	0.29%	24.09	25.52	19.44	0.2175	38.38	0.1065	0.0119
I-LoRA$_{\text{AUG}}$ (multi step)	Diffusion	Open	0.17%	21.41	28.57	17.39	0.2042	41.21	0.0881	0.0099
I-LoRA (single step)	Diffusion	Open	0.17%	16.63	23.64	13.69	0.1179	52.59	0.0487	0.0118

Extending I-LoRA to DINO. I-LoRA can extend beyond generative models to include self-supervised, non-generative models like DINO (Darcet et al., 2023). To explore this possibility, albeit tangential to our main objective of extracting intrinsic knowledge from generative models, we follow Oquab et al. (2023) by learning a linear head to project DINO features to pixel space, along with our I-LoRA modules. Using DINOv2's "giant" model, we achieve quantitative results on par with our I-LoRA at the cost of only 0.26% extra parameters. However, qualitatively, DINOv2 produces less smooth intrinsics (Fig. 7d) with apparent discontinuities. This broad applicability echoes Bhattad et al. (2023a)'s "meaningful image representations are those that can capture these intrinsic properties", a hypothesis validated across models of various types.

Table 3: Quantitative analysis of scene intrinsic extraction performance across different models on real images.

Model	Pre-training	LoRA	Surface Normal			Depth	
	Type	Param	Mean Error°↓	Median Error°↓	L1 Error$_{\times 100}$ ↓	RMS ↓	$\delta < 1.25_{\times 100}$ ↑
Omnidata-v2 (Kar et al., 2022)/ZoeDepth (Bhat et al., 2023)	Supervised	-	**18.90**	13.36	**15.21**	0.2693	**47.56**
DINOv2	Non-Generative	0.26%	19.74	13.72	16.00	0.2094	44.32
I-LoRA$_{\text{AUG}}$ (multi step)	Diffusion	0.17%	23.74	19.08	19.31	0.2651	43.19
I-LoRA (single step)	Diffusion	0.17%	20.31	**12.54**	16.53	**0.2046**	44.90

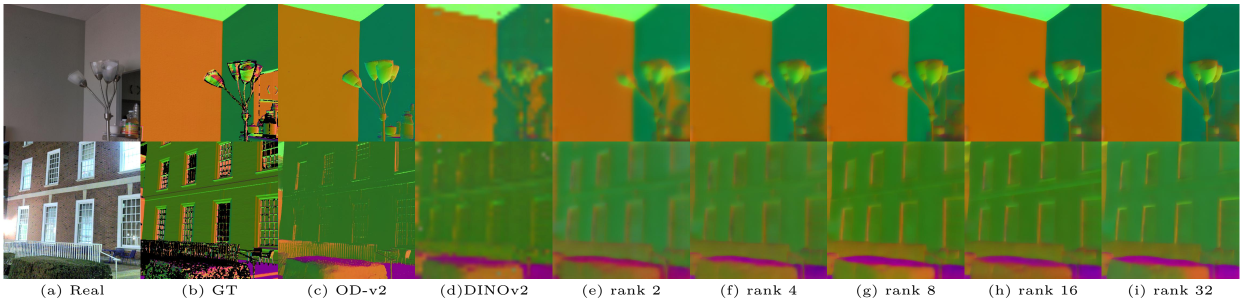

(a) Real (b) GT (c) OD-v2 (d)DINOv2 (e) rank 2 (f) rank 4 (g) rank 8 (h) rank 16 (i) rank 32

	(c) OD-v2	(d)DINOv2	(e) rank 2	(f) rank 4	(g) rank 8	(h) rank 16	(i) rank 32
Mean Angular Error°↓	18.90	19.74	22.28	22.57	20.31	21.17	21.84
L1 Error (× 100)↓	15.21	16.00	18.14	18.39	16.53	17.19	17.81
LoRA Param.	-	0.26%	0.04%	0.08%	0.17%	0.34%	0.68%

Figure 7: Parameter Efficiency of I-LoRA. We evaluate I-LoRA across various rank settings for surface normal extraction. Lower ranks such as 8 offer a balance between efficiency and effectiveness. All model variants are trained using SD's UNet (v1.5) with 4000 samples. Performance metrics, such as Mean Angular Error and L1 Error for normals, and additional parameter counts are detailed below each variant.

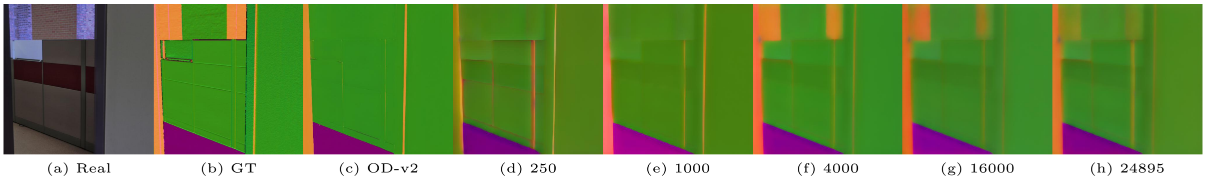

(a) Real (b) GT (c) OD-v2 (d) 250 (e) 1000 (f) 4000 (g) 16000 (h) 24895

	(c) OD-v2	(d) 250	(e) 1000	(f) 4000	(g) 16000	(h) 24895
Mean Angular Error°↓	18.90	27.73	22.22	20.31	21.26	21.64
L1 Error (× 100) ↓	15.21	22.46	18.05	16.53	17.33	17.64

Figure 8: Data efficiency of I-LoRA. Note: SOTA supervised model (c), was trained using 12M+ labeled training samples. Even with 250 samples, I-LoRA captures surface normals. We observe the best performance with 4k samples. Models (d)-(h) all use the same SD UNet(v1-5) and rank 8 LoRA.

4.2 I-LoRA is Parameter and Label Efficient

Our single-step I-LoRA model, distinguished by its high quantitative performance, serves as the basis for ablation studies that assess the influence of rank and labeled data quantity on intrinsic extraction efficiency. We verify that the requirements for compute, parameters, and data to learn I-LoRA are minimal.

Parameter efficiency. Fig. 7 shows surface normal predictions across LoRA ranks. The highest accuracy is achieved with Rank 8, balancing accuracy and memory. Notably, a Rank 2 LoRA with only 0.4M additional parameters (a mere 0.04% increase) still yields good performance. Note that across different generative models, Rank 8 adaptors adds only 0.17% to 0.57% additional parameters (Tab. 2).
Label efficiency. The impact of the labeled data size is analyzed in Fig. 8. I-LoRA reaches peak performance using a modest 4000 training examples, with credible predictions visible from as few as 250 samples.

4.3 Control Experiments and Correlation with Generative Quality

To assess if our I-LoRA leverages pre-trained generative capabilities or primarily depends on LoRA layers, we performed a control experiment using a randomly initialized SD UNet, following the same training protocol of our I-LoRA model. The poor results from this model (see Fig. 9) corroborate that the learned features developed during generative pre-training are crucial for intrinsic extraction, rather than I-LoRA layers

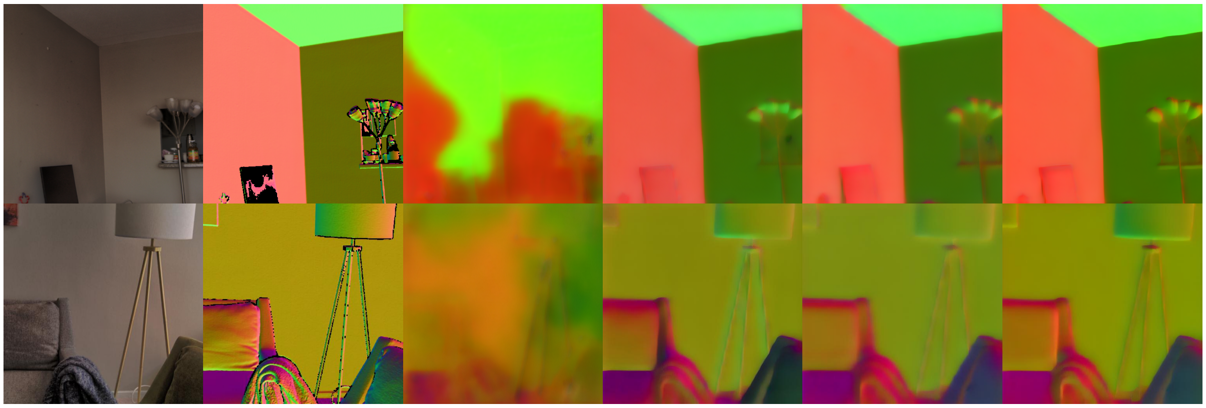

Real	GT	Random init.	I-LoRA v1-1	I-LoRA v1-2	I-LoRA v1-5
Mean Angular Error°↓		36.18	21.84	21.41	20.31
L1 Error (× 100) ↓		29.28	17.78	17.38	16.53

Figure 9: We find a correlation between generative model quality and scene intrinsic extraction accuracy. We compare different versions of Stable Diffusion (v1-1, v1-2, v1-5). The progress from SD v1-1 to SD v1-5 shows improvements in intrinsic extraction paralleling improvements in image generation. Control experiments with a randomly initialized UNet fail to extract surface normals, emphasizing the reliance on learned priors from generative training for effective intrinsic representation extraction.

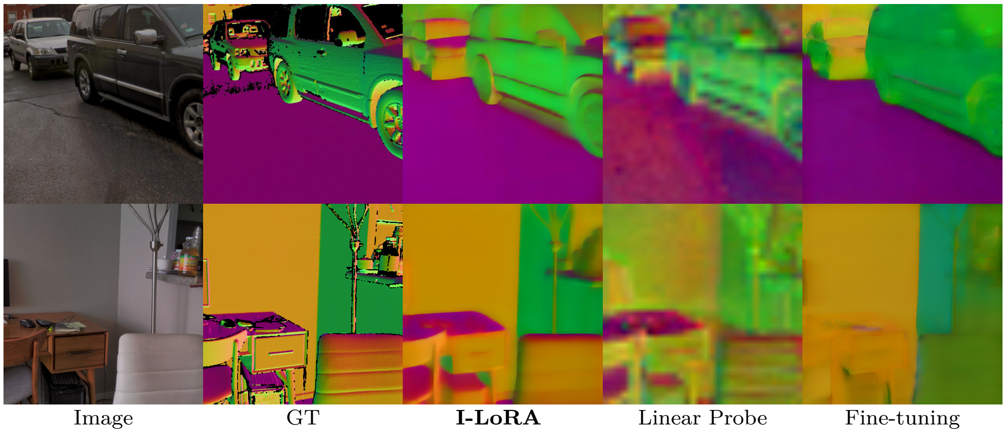

Figure 10: Comparison with baselines. All models are trained with 250 samples. Note LoRA effectively extracts better normals compared to other baselines.

Table 4: We find I-LoRA to consistently outperform baselines for different training samples (first row).

	Steps/s	Peak Train GPU Mem%	250		1000		4000		16000	
			Mean Error°↓	L1 $\times$ 100 ↓	Mean Error°↓	L1 $\times$ 100 ↓	Mean Error°↓	L1 $\times$ 100 ↓	Mean Error°↓	L1 $\times$ 100 ↓
Linear Probe	2.13	29.46%	29.10	23.74	28.45	23.25	28.52	23.26	28.22	23.11
Fine-tuning	0.77	86.78%	34.40	27.58	25.19	20.28	28.03	22.17	27.39	22.24
LoRA (Ours)	0.94	63.48%	**27.73**	**22.46**	**22.22**	**18.05**	**20.31**	**16.53**	**21.26**	**17.33**

alone. Furthermore, analyzing multiple Stable Diffusion versions (v1-1, v1-2 and v1-5) under the same I-LoRA protocol reveals that enhancements in image generation quality correlate positively with intrinsic extraction capabilities. This assertion is further reinforced by observing a correlation between lower FID scores (9.6 for VQGAN (Esser et al., 2020), 3.62 for StyleGAN-v2 (Karras et al., 2020a) and 2.19 for StyleGAN-XL (Sauer et al., 2022)) and improved intrinsic predictions in our FFHQ experiments (Fig. 3 and Tab. 2: first three rows), confirming that superior generative models yield more accurate intrinsics.

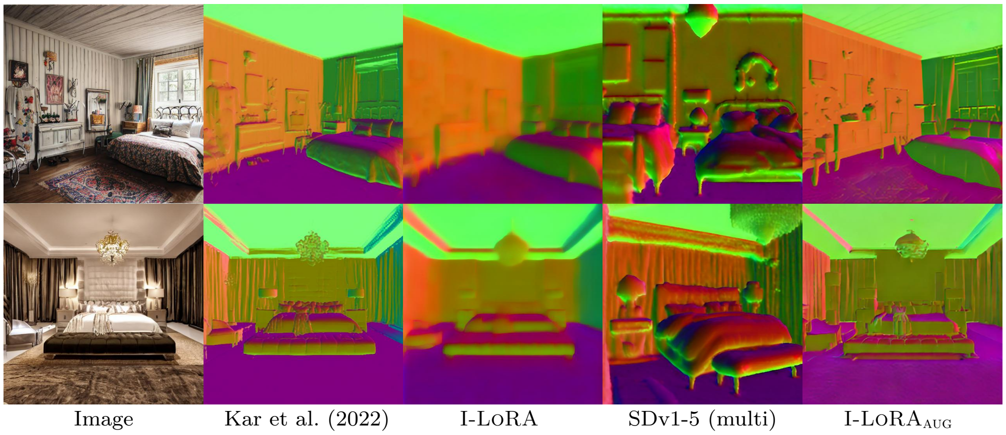

Figure 11: I-LoRA yields satisfactory results, but multiple diffusion steps lead to misalignment in extracted intrinsics (fourth column). The last column, I-LoRA$_{\text{AUG}}$, demonstrates successfully correcting the misalignment using our image conditioning approach, resulting in well-aligned and detailed intrinsic extractions

4.4 Superiority of I-LoRA over Fine-tuning and Linear Probing

We compare I-LoRA with two common baselines: linear probing and full model fine-tuning. Following Chen et al. (2023) for linear probing and employing standard fine-tuning practices, we train all methods with a small dataset of 250 samples to 16000 samples. All three models are trained with the same number of epochs and have converged at the end of the training. Our findings in Tab. 4 and Fig. 10 show that I-LoRA significantly outperforms these baselines in low-data regimes, validating its superior efficacy and data efficiency.

5 I-LoRA$_{\text{aug}}$: Towards Improved Intrinsic Extraction

In the previous section, we showed that Stable Diffusion models inherently capture various scene intrinsics like normals, depth, albedo, and shading, as evidenced by our evaluation of I-LoRA . A natural question arises: can we enhance these intrinsics using multi-step diffusion inference? While multi-step diffusion improves sharpness, we find it introduces two challenges: 1. intrinsics misaligned with input, and 2. shift in the distribution of outputs relative to the ground truth (visually manifesting as a color shift) (see Fig. 11).

To address the first challenge, we augment the noise input to the UNet with the input image's latent encoding, as in InstructPix2Pix (Brooks et al., 2023). The second challenge is a known artifact attributed to Stable Diffusion's difficulty generating images that are not with medium brightness (Deck & Bischoff, 2023; Lin et al., 2023). Lin et al. (2023) propose a Zero SNR strategy that reduces color discrepancies but requires diffusion models trained with v-prediction objective, which SDv1-5 does not. However, Stable Diffusion v2-1 employs a v-prediction objective. Therefore we replace SDv1-5 with SDv2-1 while maintaining our previously described learning protocol. We name this multi-step augmented SDv2-1 model I-LoRA$_{\text{AUG}}$. I-LoRA$_{\text{AUG}}$ solves the misalignment issue and reduces the color shift significantly (Fig. 12), resulting in the generation of high-quality, sharp scene intrinsics with improved quantitative accuracy. However, quantitatively, the results still fall short of our single-step I-LoRA result. In the future, we hope this problem will be solved by improved sampling techniques and the next generation of generative models.

6 Discussions, Limitations and Broader Impact

We find consistent evidence that generative models implicitly learn physical scene intrinsics, allowing tiny LoRA adaptors to extract this information with minimal fine-tuning on small labeled data. More powerful generative models produce more accurate scene intrinsics, strengthening our hypothesis that learning this information is a natural byproduct of learning to generate images well. Additionally, we discovered scene intrinsics exist across generative models and the self-supervised DINOv2, resonating with Barrow & Tenenbaum (1978)'s hypothesis of fundamental "scene characteristics" emerging in visual processing.

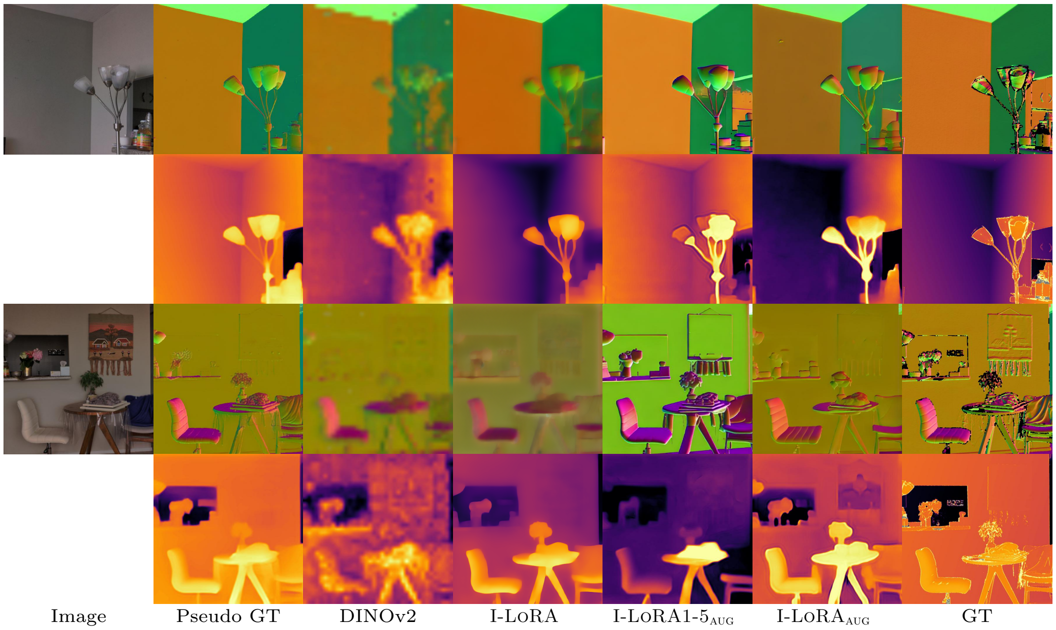

Figure 12: We show normals (top in each set) and depth (bottom in each set) derived from improved multi-step diffusion process from our I-LoRA$_{\text{AUG}}$ compared with other alternatives. I-LoRA1-5$_{\text{AUG}}$ is similar to I-LoRA$_{\text{AUG}}$ except it uses SDv1-5 and does not use Zero SNR strategy. I-LoRA1-5$_{\text{AUG}}$ presents sharper details, especially in complex areas – structures like lamp stand and chair. I-LoRA$_{\text{AUG}}$, on the other hand, illustrates a significant improvement in reducing color shifts while maintaining sharpness, as seen in the comparison with ground truth in the last column.

Our approach shows that models can generate intrinsic images directly from the same decoder head, despite these images being out-of-distribution and unlike real images. Surprisingly, it is easy to extract this information using our method, which is broadly applicable across generative models, supporting our argument that these representations are indeed inherent in the learned model.

Limitations. Although we have demonstrated that generative models carry a wealth of intrinsic information, it is still ambiguous how these models use this information when generating images. Secondly, even though I-LoRA is both parameter and label-efficient, we believe there is still room for further reduction of training requirements and perhaps the development of a parameter-free approach. Lastly, the I-LoRA$_{\text{AUG}}$ generates sharper results but still lags behind its single-step counterpart in terms of quantitative analysis. Further work is needed to explore this question.

Our **future work** will focus on overcoming the limitations we have encountered so far and expanding on our findings. One way to do this is by explicitly incorporating the extracted scene intrinsics into the learning process of generative image models to improve them further via efficient fine-tuning. Additionally, developing an evaluation of generative models based on physical properties may help develop interpretable metrics. Another direction interesting to explore is learning specific latent codes similar to Bhattad et al. (2023a) for each intrinsics, as opposed to using LoRA modules, to further reduce the number of learned parameters.

Broader Impact Statement. Our paper introduces "Intrinsic LoRA", a model-agnostic framework for extracting intrinsic properties and visual knowledge from generative models. This advancement has the potential to significantly enhance the interpretability and usability of generative models across various applications, from computer vision to autonomous systems. By enabling efficient and accurate extraction of scene intrinsics, our approach could improve image generation quality and provide deeper insights into how these models understand and recreate the visual world. Furthermore, the ability to recover intrinsic information with minimal data and computational resources promotes more sustainable and accessible AI research and development. Finally, our work contributes to the foundational understanding of generative models, paving the way for more responsible, transparent and effective AI systems in the future.

References

Rameen Abdal, Peihao Zhu, Niloy J Mitra, and Peter Wonka. Labels4free: Unsupervised segmentation using stylegan. In Proceedings of the IEEE/CVF International Conference on Computer Vision, 2021.

Zhipeng Bao, Martial Hebert, and Yu-Xiong Wang. Generative modeling for multi-task visual learning. In International Conference on Machine Learning. PMLR, 2022.

H Barrow and J Tenenbaum. Recovering intrinsic scene characteristics. Comput. vis. syst, 1978.

David Bau, Jun-Yan Zhu, Hendrik Strobelt, Agata Lapedriza, Bolei Zhou, and Antonio Torralba. Understanding the role of individual units in a deep neural network. Proceedings of the National Academy of Sciences, 2020.

Yonatan Belinkov and James Glass. Analysis methods in neural language processing: A survey. Transactions of the Association for Computational Linguistics, 7:49–72, 2019.

Shariq Farooq Bhat, Reiner Birkl, Diana Wofk, Peter Wonka, and Matthias Müller. Zoedepth: Zero-shot transfer by combining relative and metric depth. arXiv preprint arXiv:2302.12288, 2023.

Anand Bhattad and David A Forsyth. Cut-and-paste object insertion by enabling deep image prior for reshading. In 2022 International Conference on 3D Vision (3DV). IEEE, 2022.

Anand Bhattad, Daniel McKee, Derek Hoiem, and DA Forsyth. Stylegan knows normal, depth, albedo, and more. In Advances in Neural Information Processing Systems (NeurIPS), 2023a.

Anand Bhattad, Viraj Shah, Derek Hoiem, and DA Forsyth. Make it so: Steering stylegan for any image inversion and editing. arXiv preprint arXiv:2304.14403, 2023b.

Anand Bhattad, James Soole, and DA Forsyth. Stylitgan: Image-based relighting via latent control. In Proceedings of the IEEE/CVF Conference on Computer Vision and Pattern Recognition, pp. 4231–4240, 2024.

Tim Brooks, Aleksander Holynski, and Alexei A Efros. Instructpix2pix: Learning to follow image editing instructions. In Proceedings of the IEEE/CVF Conference on Computer Vision and Pattern Recognition, 2023.

Yida Chen, Fernanda Viégas, and Martin Wattenberg. Beyond surface statistics: Scene representations in a latent diffusion model. arXiv preprint arXiv:2306.05720, 2023.

Timothée Darcet, Maxime Oquab, Julien Mairal, and Piotr Bojanowski. Vision transformers need registers. arXiv preprint arXiv:2309.16588, 2023.

Katherine Deck and Tobias Bischoff. Easing color shifts in score-based diffusion models. arXiv preprint arXiv:2306.15832, 2023.

Jia Deng, Wei Dong, Richard Socher, Li-Jia Li, Kai Li, and Li Fei-Fei. Imagenet: A large-scale hierarchical image database. In 2009 IEEE conference on computer vision and pattern recognition. Ieee, 2009.

Ainaz Eftekhar, Alexander Sax, Jitendra Malik, and Amir Zamir. Omnidata: A scalable pipeline for making multi-task mid-level vision datasets from 3d scans. In Proceedings of the IEEE/CVF International Conference on Computer Vision, 2021.

David Eigen, Christian Puhrsch, and Rob Fergus. Depth map prediction from a single image using a multi-scale deep network. Advances in neural information processing systems, 2014.

Patrick Esser, Robin Rombach, and Björn Ommer. Taming transformers for high-resolution image synthesis, 2020.

Allyson Ettinger. What bert is not: Lessons from a new suite of psycholinguistic diagnostics for language models. Transactions of the Association for Computational Linguistics, 8:34–48, 2020.

David Forsyth and Jason J Rock. Intrinsic image decomposition using paradigms. IEEE transactions on pattern analysis and machine intelligence, 2021.

Rinon Gal, Yuval Alaluf, Yuval Atzmon, Or Patashnik, Amit Haim Bermano, Gal Chechik, and Daniel Cohen-or. An image is worth one word: Personalizing text-to-image generation using textual inversion. In The Eleventh International Conference on Learning Representations, 2022.

Yulu Gan, Sungwoo Park, Alexander Schubert, Anthony Philippakis, and Ahmed Alaa. Instructcv: Instruction-tuned text-to-image diffusion models as vision generalists. arXiv preprint arXiv:2310.00390, 2023.

Ian Goodfellow, Jean Pouget-Abadie, Mehdi Mirza, Bing Xu, David Warde-Farley, Sherjil Ozair, Aaron Courville, and Yoshua Bengio. Generative adversarial nets. Advances in neural information processing systems, 27, 2014.

Michael Gutmann and Aapo Hyvärinen. Noise-contrastive estimation: A new estimation principle for unnormalized statistical models. In Proceedings of the thirteenth international conference on artificial intelligence and statistics. JMLR Workshop and Conference Proceedings, 2010.

Eric Hedlin, Gopal Sharma, Shweta Mahajan, Hossam Isack, Abhishek Kar, Andrea Tagliasacchi, and Kwang Moo Yi. Unsupervised semantic correspondence using stable diffusion. arXiv preprint arXiv:2305.15581, 2023.

Jonathan Ho, Ajay Jain, and Pieter Abbeel. Denoising diffusion probabilistic models. Advances in neural information processing systems, 2020.

Edward J Hu, Yelong Shen, Phillip Wallis, Zeyuan Allen-Zhu, Yuanzhi Li, Shean Wang, Lu Wang, and Weizhu Chen. LoRA: Low-rank adaptation of large language models. In International Conference on Learning Representations, 2022.

Ali Jahanian, Xavier Puig, Yonglong Tian, and Phillip Isola. Generative models as a data source for multiview representation learning. arXiv preprint arXiv:2106.05258, 2021.

Minguk Kang, Jun-Yan Zhu, Richard Zhang, Jaesik Park, Eli Shechtman, Sylvain Paris, and Taesung Park. Scaling up gans for text-to-image synthesis. In Proceedings of the IEEE Conference on Computer Vision and Pattern Recognition (CVPR), 2023.

Oğuzhan Fatih Kar, Teresa Yeo, Andrei Atanov, and Amir Zamir. 3d common corruptions and data augmentation. In Proceedings of the IEEE/CVF Conference on Computer Vision and Pattern Recognition, 2022.

Tero Karras, Samuli Laine, and Timo Aila. A style-based generator architecture for generative adversarial networks. In Proceedings of the IEEE/CVF Conference on Computer Vision and Pattern Recognition, 2019.

Tero Karras, Miika Aittala, Janne Hellsten, Samuli Laine, Jaakko Lehtinen, and Timo Aila. Training generative adversarial networks with limited data. In Proc. NeurIPS, 2020a.

Tero Karras, Samuli Laine, Miika Aittala, Janne Hellsten, Jaakko Lehtinen, and Timo Aila. Analyzing and improving the image quality of stylegan. In Proceedings of the IEEE/CVF Conference on Computer Vision and Pattern Recognition, 2020b.

Tero Karras, Miika Aittala, Timo Aila, and Samuli Laine. Elucidating the design space of diffusion-based generative models. Advances in Neural Information Processing Systems, 2022.

Bingxin Ke, Anton Obukhov, Shengyu Huang, Nando Metzger, Rodrigo Caye Daudt, and Konrad Schindler. Repurposing diffusion-based image generators for monocular depth estimation. arXiv preprint arXiv:2312.02145, 2023.

Hsin-Ying Lee, Hung-Yu Tseng, Hsin-Ying Lee, and Ming-Hsuan Yang. Exploiting diffusion prior for generalizable pixel-level semantic prediction. arXiv preprint arXiv:2311.18832, 2023.

Daiqing Li, Junlin Yang, Karsten Kreis, Antonio Torralba, and Sanja Fidler. Semantic segmentation with generative models: Semi-supervised learning and strong out-of-domain generalization. In Proceedings of the IEEE/CVF Conference on Computer Vision and Pattern Recognition, 2021.

Shanchuan Lin, Bingchen Liu, Jiashi Li, and Xiao Yang. Common diffusion noise schedules and sample steps are flawed. arXiv preprint arXiv:2305.08891, 2023.

Jonathan Long, Evan Shelhamer, and Trevor Darrell. Fully convolutional networks for semantic segmentation. In Proceedings of the IEEE conference on computer vision and pattern recognition, 2015.

Cheng Lu, Yuhao Zhou, Fan Bao, Jianfei Chen, Chongxuan Li, and Jun Zhu. Dpm-solver++: Fast solver for guided sampling of diffusion probabilistic models. arXiv preprint arXiv:2211.01095, 2022.

Grace Luo, Trevor Darrell, Oliver Wang, Dan B Goldman, and Aleksander Holynski. Readout guidance: Learning control from diffusion features. arXiv preprint arXiv:2312.02150, 2023a.

Grace Luo, Lisa Dunlap, Dong Huk Park, Aleksander Holynski, and Trevor Darrell. Diffusion hyperfeatures: Searching through time and space for semantic correspondence. In Advances in Neural Information Processing Systems, 2023b.

Chenlin Meng, Yutong He, Yang Song, Jiaming Song, Jiajun Wu, Jun-Yan Zhu, and Stefano Ermon. Sdedit: Guided image synthesis and editing with stochastic differential equations. In International Conference on Learning Representations, 2021.

Thao Nguyen, Yuheng Li, Utkarsh Ojha, and Yong Jae Lee. Visual instruction inversion: Image editing via visual prompting. arXiv preprint arXiv:2307.14331, 2023.

Atsuhiro Noguchi and Tatsuya Harada. Rgbd-gan: Unsupervised 3d representation learning from natural image datasets via rgbd image synthesis. In International Conference on Learning Representations, 2020.

Maxime Oquab, Timothée Darcet, Théo Moutakanni, Huy Vo, Marc Szafraniec, Vasil Khalidov, Pierre Fernandez, Daniel Haziza, Francisco Massa, Alaaeldin El-Nouby, et al. Dinov2: Learning robust visual features without supervision. arXiv preprint arXiv:2304.07193, 2023.

Xingang Pan, Bo Dai, Ziwei Liu, Chen Change Loy, and Ping Luo. Do 2d gans know 3d shape? unsupervised 3d shape reconstruction from 2d image gans. In International Conference on Learning Representations, 2021.

Dustin Podell, Zion English, Kyle Lacey, Andreas Blattmann, Tim Dockhorn, Jonas Müller, Joe Penna, and Robin Rombach. Sdxl: Improving latent diffusion models for high-resolution image synthesis. arXiv preprint arXiv:2307.01952, 2023.

René Ranftl, Alexey Bochkovskiy, and Vladlen Koltun. Vision transformers for dense prediction. In Proceedings of the IEEE/CVF International Conference on Computer Vision, 2021.

Ali Razavi, Aaron Van den Oord, and Oriol Vinyals. Generating diverse high-fidelity images with vq-vae-2. Advances in neural information processing systems, 32, 2019.

Robin Rombach, Andreas Blattmann, Dominik Lorenz, Patrick Esser, and Björn Ommer. High-resolution image synthesis with latent diffusion models. In Proceedings of the IEEE/CVF Conference on Computer Vision and Pattern Recognition, 2022.

Chitwan Saharia, William Chan, Saurabh Saxena, Lala Li, Jay Whang, Emily L Denton, Kamyar Ghasemipour, Raphael Gontijo Lopes, Burcu Karagol Ayan, Tim Salimans, et al. Photorealistic text-to-image diffusion models with deep language understanding. Advances in Neural Information Processing Systems, 2022.

Mert Bulent Sariyildiz, Karteek Alahari, Diane Larlus, and Yannis Kalantidis. Fake it till you make it: Learning transferable representations from synthetic imagenet clones. In CVPR 2023–IEEE/CVF Conference on Computer Vision and Pattern Recognition, 2023.

Ayush Sarkar, Hanlin Mai, Amitabh Mahapatra, Svetlana Lazebnik, and Anand Bhattad. Shadows don't lie and lines can't bend! generative models don't know projective geometry... for now. arXiv preprint arXiv:2311.17138, 2023.

Axel Sauer, Katja Schwarz, and Andreas Geiger. Stylegan-xl: Scaling stylegan to large diverse datasets. In ACM SIGGRAPH 2022 conference proceedings, 2022.

Luming Tang, Menglin Jia, Qianqian Wang, Cheng Perng Phoo, and Bharath Hariharan. Emergent correspondence from image diffusion. arXiv preprint arXiv:2306.03881, 2023.

Aaron Van den Oord, Nal Kalchbrenner, Lasse Espeholt, Oriol Vinyals, Alex Graves, et al. Conditional image generation with pixelcnn decoders. Advances in neural information processing systems, 29, 2016.

Aäron Van Den Oord, Nal Kalchbrenner, and Koray Kavukcuoglu. Pixel recurrent neural networks. In International conference on machine learning. PMLR, 2016.

Igor Vasiljevic, Nick Kolkin, Shanyi Zhang, Ruotian Luo, Haochen Wang, Falcon Z Dai, Andrea F Daniele, Mohammadreza Mostajabi, Steven Basart, Matthew R Walter, et al. Diode: A dense indoor and outdoor depth dataset. arXiv preprint arXiv:1908.00463, 2019.

Pascal Vincent. A connection between score matching and denoising autoencoders. Neural computation, 2011.

Weijia Wu, Yuzhong Zhao, Hao Chen, Yuchao Gu, Rui Zhao, Yefei He, Hong Zhou, Mike Zheng Shou, and Chunhua Shen. Datasetdm: Synthesizing data with perception annotations using diffusion models. Thirty-seventh Conference on Neural Information Processing Systems (NeurIPS 2023), 2023.

Zongze Wu, Dani Lischinski, and Eli Shechtman. Stylespace analysis: Disentangled controls for stylegan image generation. In Proceedings of the IEEE/CVF Conference on Computer Vision and Pattern Recognition, 2021.

Jiarui Xu, Sifei Liu, Arash Vahdat, Wonmin Byeon, Xiaolong Wang, and Shalini De Mello. Open-Vocabulary Panoptic Segmentation with Text-to-Image Diffusion Models. arXiv preprint arXiv:2303.04803, 2023.

Ceyuan Yang, Yujun Shen, and Bolei Zhou. Semantic hierarchy emerges in deep generative representations for scene synthesis. International Journal of Computer Vision, 2021.

Fisher Yu, Ari Seff, Yinda Zhang, Shuran Song, Thomas Funkhouser, and Jianxiong Xiao. Lsun: Construction of a large-scale image dataset using deep learning with humans in the loop. arXiv preprint arXiv:1506.03365, 2015.

Jiahui Yu, Yuanzhong Xu, Jing Yu Koh, Thang Luong, Gunjan Baid, Zirui Wang, Vijay Vasudevan, Alexander Ku, Yinfei Yang, Burcu Karagol Ayan, Ben Hutchinson, Wei Han, Zarana Parekh, Xin Li, Han Zhang, Jason Baldridge, and Yonghui Wu. Scaling autoregressive models for content-rich text-to-image generation. Transactions on Machine Learning Research, 2022. ISSN 2835-8856.

Lili Yu, Bowen Shi, Ramakanth Pasunuru, Benjamin Muller, Olga Golovneva, Tianlu Wang, Arun Babu, Binh Tang, Brian Karrer, Shelly Sheynin, et al. Scaling autoregressive multi-modal models: Pretraining and instruction tuning. arXiv preprint arXiv:2309.02591, 2023.

Ning Yu, Guilin Liu, Aysegul Dundar, Andrew Tao, Bryan Catanzaro, Larry S Davis, and Mario Fritz. Dual contrastive loss and attention for gans. In Proceedings of the IEEE/CVF International Conference on Computer Vision, 2021.

Ye Yu and William AP Smith. Inverserendernet: Learning single image inverse rendering. In Proceedings of the IEEE Conference on Computer Vision and Pattern Recognition, 2019.

Guanqi Zhan, Chuanxia Zheng, Weidi Xie, and Andrew Zisserman. What does stable diffusion know about the 3d scene? arXiv preprint arXiv:2310.06836, 2023.

Yuxuan Zhang, Wenzheng Chen, Huan Ling, Jun Gao, Yinan Zhang, Antonio Torralba, and Sanja Fidler. Image gans meet differentiable rendering for inverse graphics and interpretable 3d neural rendering. In International Conference on Learning Representations, 2021a.

Yuxuan Zhang, Huan Ling, Jun Gao, Kangxue Yin, Jean-Francois Lafleche, Adela Barriuso, Antonio Torralba, and Sanja Fidler. Datasetgan: Efficient labeled data factory with minimal human effort. In Proceedings of the IEEE/CVF Conference on Computer Vision and Pattern Recognition, 2021b.

Wenliang Zhao, Yongming Rao, Zuyan Liu, Benlin Liu, Jie Zhou, and Jiwen Lu. Unleashing text-to-image diffusion models for visual perception. ICCV, 2023.

A Additional Ablation Studies

A.1 Number of Diffusion Steps

Mean Angular Error°↓	25.83	23.79	23.48	23.86	23.79	23.74	23.67
L1 Error (× 100) ↓	21.08	19.39	19.10	19.40	19.35	19.31	19.25

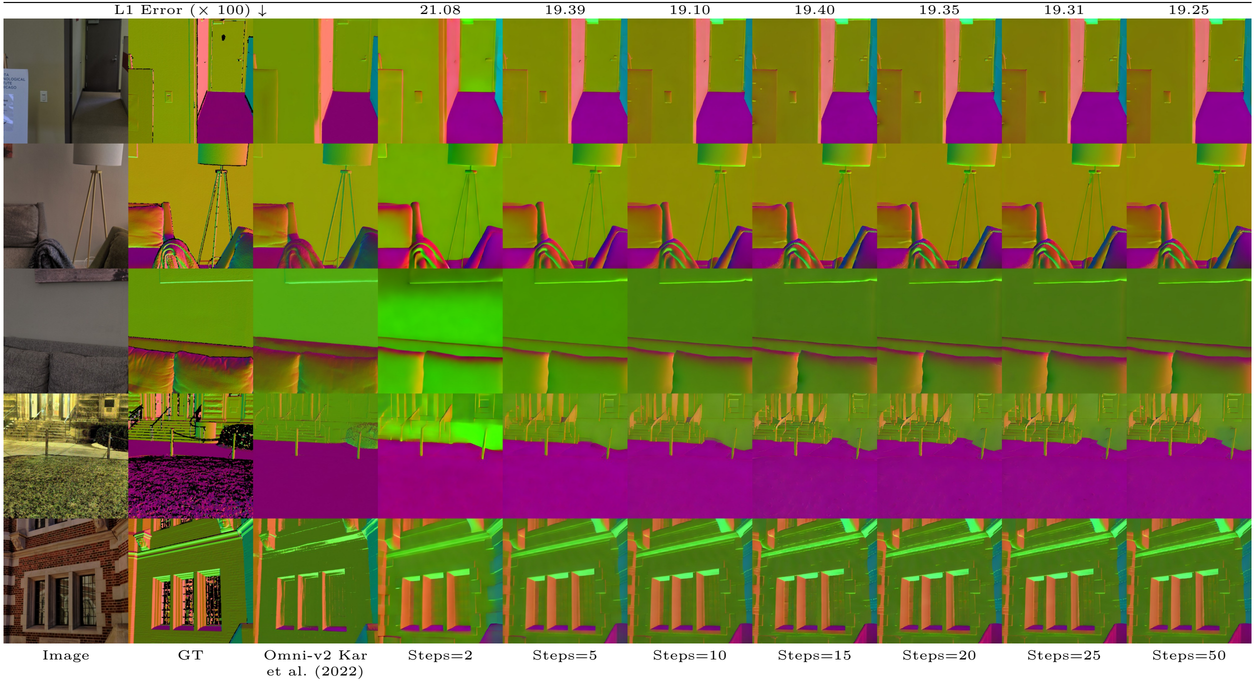

Figure 13: Ablation study to determine the effect of varying numbers of diffusion steps while keeping CFG fixed at 3.0. Our findings show that there are very small differences, both in terms of quantity and quality, after 10 steps. For our main paper, we report results for 25 steps as it is more stable across different intrinsics.

To assess the impact of the number of diffusion steps on the performance of the multi-step I-LoRA$_{\text{AUG}}$ model, we conducted an ablation study. The results are presented in Fig. 13. For all our experiments in the main text, we used DPMSolver++ (Lu et al., 2022). Interestingly, the quality of results did not vary significantly with an increased number of steps, indicating that 10 steps are sufficient for extracting better surface normals from the Stable Diffusion. Nevertheless, we use 25 steps for all our experiments because it is more stable across different image intrinsics.

A.2 CFG scales

When working with the multi-step I-LoRA$_{\text{AUG}}$, the quality of the final output is influenced by the choice of classifier-free guidance (CFG) scales during the inference process. In Fig. 14, we present a comparison of the effects of using different CFG scales. Based on our experiments, we found that using CFG=3.0 results in the best overall quality and minimizes color-shift artifacts.

B Other Ablations and Baselines

We extensively study the effect of applying LoRA to different attention layers within Stable Diffusion models. Specifically, we investigate the outcomes of targeting up-blocks, mid-block, down-blocks, cross-attention, and self-attention layers individually. We find (Fig. 15) that isolating LoRA to up or down blocks or the mid-block alone is less effective or diverges, and applying to either cross- or self-attention layers yields decent results, though combining them is best.

Mean Angular Error°↓	24.28	23.48	25.72	27.80	29.85	31.93	34.12
L1 Error (× 100) ↓	19.48	19.10	21.01	22.72	24.36	26.03	27.78

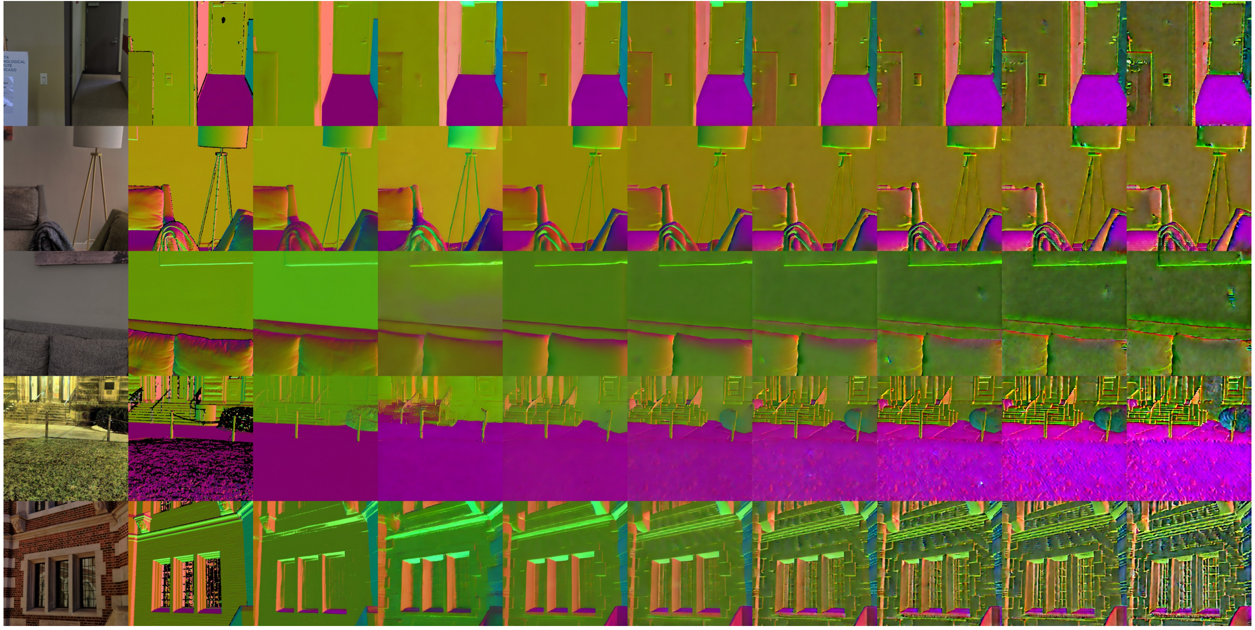

Figure 14: Ablation study analyzing the impact of different classifier-free guidance (CFG) on I-LoRA$_{\text{AUG}}$ surface normal prediction. For efficiency, we experimented with a step of 10. We observed that CFG=1 sometimes led to incorrect semantic predictions, particularly in the case of stairs in row 4. On the other hand, using large CFGs (5 and beyond) results in more severe color shift problems.

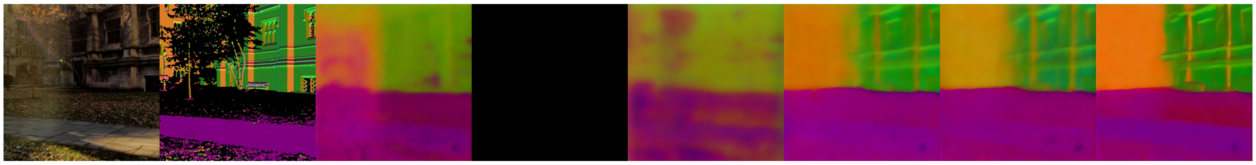

	Up blocks	Mid block	Down blocks	Cross-attn	Self-attn	All
Mean Angular Error°↓	32.25	-	36.71	23.72	21.70	20.31
L1 Error (× 100) ↓	26.10	-	29.95	19.27	17.69	16.53

Figure 15: Ablation study on the effect of applying LoRA on different types of attention layers. We started all models with SD v1-5, 4000 training samples and LoRA rank=8. Training with LoRA only on the mid block never converges.

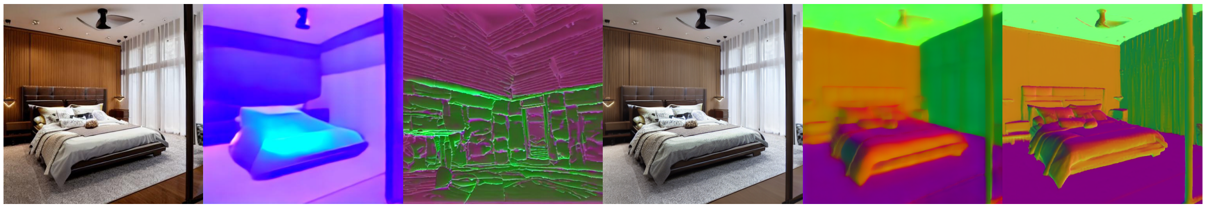
Image
VISII (Nguyen et al., 2023)
Text. Invers. (Gal et al., 2022)
IP2P (Brooks et al., 2023)
I-LoRA
Pseudo GT

Figure 16: Comparison of image editing techniques for surface normal mapping. VISII and Textual Inversion yield unsatisfactory results, while InstructPix2Pix fails to interpret the task, resulting in near-original output.

Additionally, we evaluated other image editing methods such as Textual Inversion (Gal et al., 2022) and VISII (Nguyen et al., 2023), alongside InstructPix2Pix's response to "Turn it into a surface normal map"

Table 5: Comparison of quality of normals extracted from StyleGAN Bhattad et al. (2023a).

	Mean Error°↓	Median Error°↓	L1 × 100 ↓
"StyleGAN knows" (Bhattad et al., 2023a)	19.92	46.65	16.64
I-LoRA-StyleGAN (Ours)	**13.24**	**23.55**	**10.92**

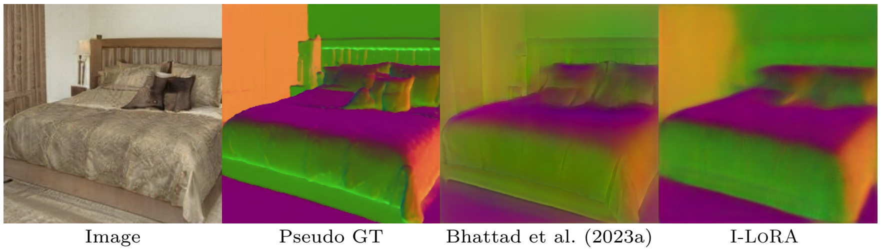

Figure 17: Qualitative results of normals extracted from StyleGAN by Bhattad et al. (2023a) and Ours.

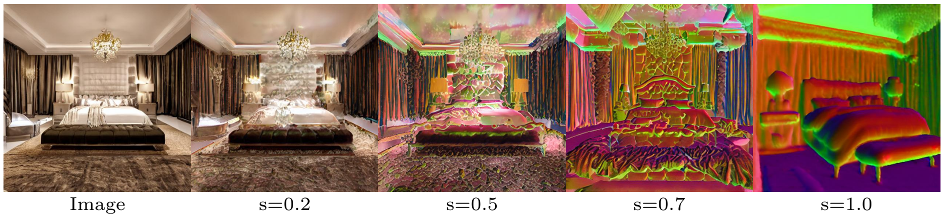

Figure 18: We observe applying SDEdit method on the SDv1-5 model alone, without incorporating the additional input image latent encoding, fails to produce satisfactorily aligned and high-quality scene intrinsics. The reason for this might be the considerable domain shift that exists between RGB images and surface normal maps, which results in severe artifacts when using SDEdit. The variable "s" represents the strength of SDEdit.

instruction (Brooks et al., 2023). As shown in Fig. 16, these methods perform poorly for intrinsic image extraction, demonstrating the effectiveness of our I-LoRA approach in extracting scene intrinsics.

We also provide a comparison with Bhattad et al. (2023a) in Tab. 5 and Fig. 17. This comparison is for the same 500 randomly generated images. I-LoRA outperforms Bhattad et al. (2023a) significantly.

In addition, we show that directly applying SDEdit (Meng et al., 2021) will also fail to extract reasonable image intrinsics. We take the model from the SDv1-5 column in Fig.13 of the main paper and apply SDEdit. In Fig. 18, we show directly applying SDEdit results in severe artifacts, regardless of strength.

C Hyper-parameters

In Table 6, we show the hyperparameters we use for each model.

D Generated Images Used for Quantitative Analysis

In Tab. 2 of the main paper, we report quantitative results on synthetic images. For Autoregressive models and GANs, we first randomly sample 500 noises and use them to generate 500 RGB images. The same 500 noises will then be used to generate intrinsics with our learned LoRAs loaded. For Stable Diffusion experiments (both single-step and multi-step), we use a single dataset with 1000 synthetic images with various prompts.

The pseudo GT are obtained by applying SOTA off-the-shelf models on the RGB images.

Table 6: Hyper-parameters for each model. LR refers to the learning rate and BS refers to the batch size. Please note that the number of steps required to reach convergence reported above is for normal/depth. However, it is worth noting that albedo and shading tend to require significantly fewer steps to converge (usually half of normal/depth). Additionally, I-LoRA$_{\text{AUG}}$ (multi-step) and I-LoRA (single-step) are trained on real-world DIODE dataset, while the other models are trained on synthetic images within a specific domain. (Num. of params of VQGAN counts transformer + first stage models; Num. of params of I-LoRA$_{\text{AUG}}$ and I-LoRA counts VAE+UNet)

Model	Dataset	Resolution	Rank	LR	BS	LoRA Params	Generator Params	Convergence Steps
VQGAN	FFHQ	256	8	1e-03	1	0.13M	873.9M	$\sim$ 4000
StyleGAN-v2	FFHQ	256	8	1e-03	1	0.14M	24.8M	$\sim$ 4000
StyleGAN-v2	LSUN Bedroom	256	8	1e-03	1	0.14M	24.8M	$\sim$ 4000
StyleGAN-XL	FFHQ	256	8	1e-03	1	0.19M	67.9M	$\sim$ 4000
StyleGAN-XL	ImageNet	256	8	1e-03	1	0.19M	67.9M	$\sim$ 4000
I-LoRA$_{\text{AUG}}$ (multi step)	Open	512	8	1e-04	4	1.59M	943.2M	$\sim$ 30000
I-LoRA (single step)	Open	512	8	1e-04	4	1.59M	943.2M	$\sim$ 15000

E Additional Qualitative Results

In Fig. 19, we present more results for I-LoRA$_{\text{AUG}}$ and I-LoRA1-5$_{\text{AUG}}$. Fig. 20 shows extra results for models trained on FFHQ dataset. More examples of scene intrinsics extracted from StyleGAN-v2 trained on LSUN bedroom can be found in Fig. 21. In Fig. 22, we show results for Stable Diffusion I-LoRA (single-step) on generated images. Shown in Fig. 23 are extra results for StyleGAN-XL trained on ImageNet.

F Results on 1024^2 synthetic images

Our multi-step I-LoRA$_{\text{AUG}}$ models, although trained exclusively on 512^2 images from the DIODE dataset, demonstrate their robustness by successfully extracting intrinsic images from 1024^2 high-resolution synthetic images generated by Stable Diffusion XL (Podell et al., 2023), as shown across Figures 24 to 33

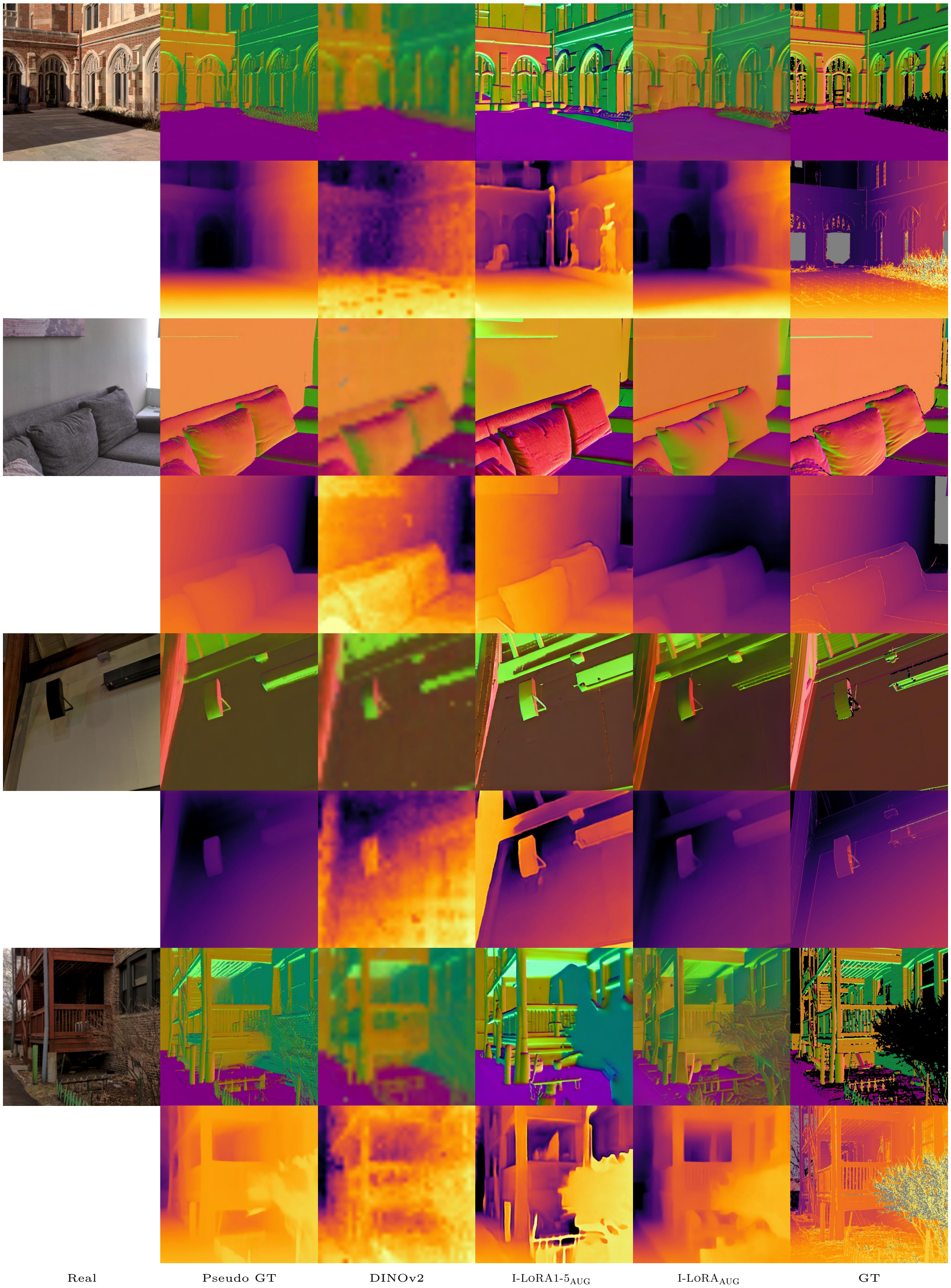

Figure 19: Additional results after applying improved diffusion techniques with I-LoRA$_{\text{AUG}}$. I-LoRA$_{\text{AUG}}$ was found to significantly reduce color shift artifacts observed in I-LoRA1-5$_{\text{AUG}}$ during the extraction of detailed scene intrinsic results.

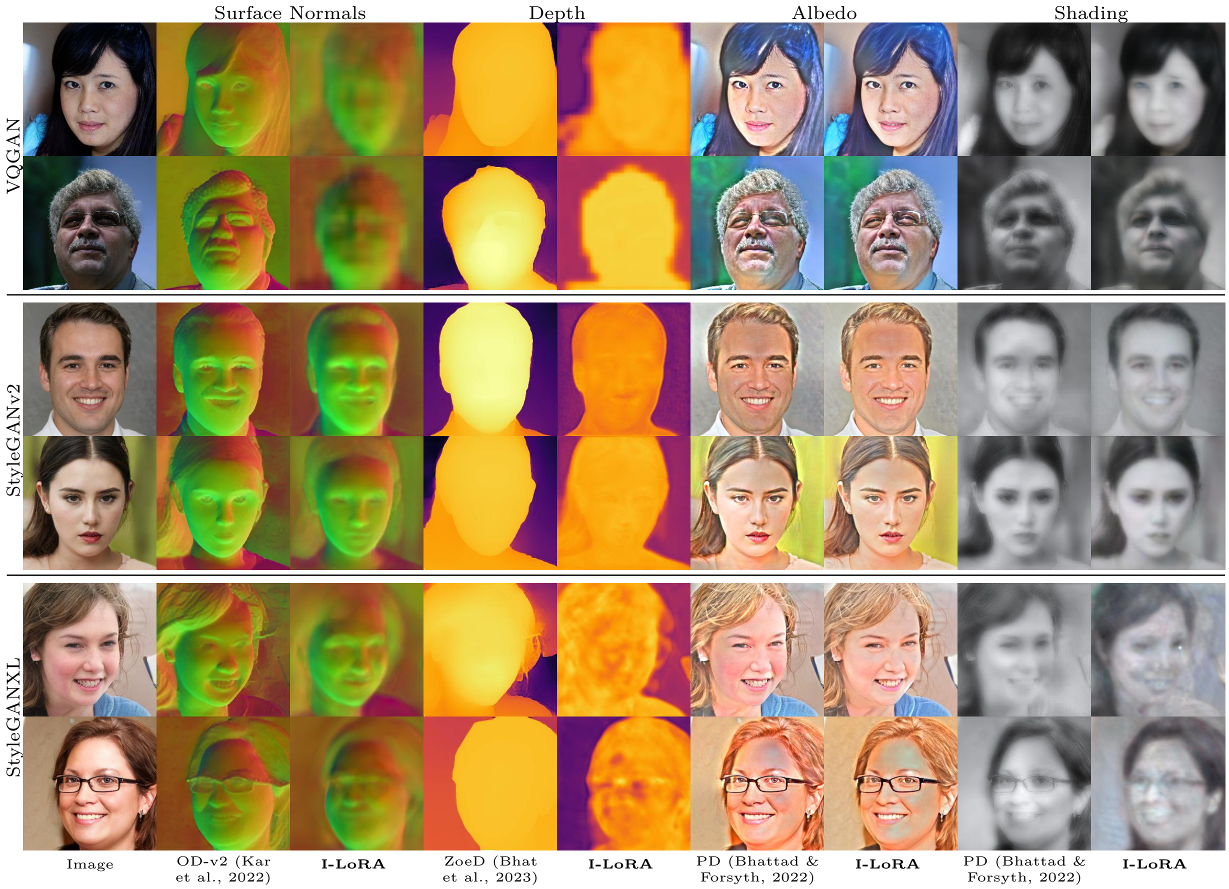

Figure 20: Additional results of scene intrinsics from different generators – VQGAN, StyleGAN-v2, and StyleGAN-XL – trained on FFHQ dataset.

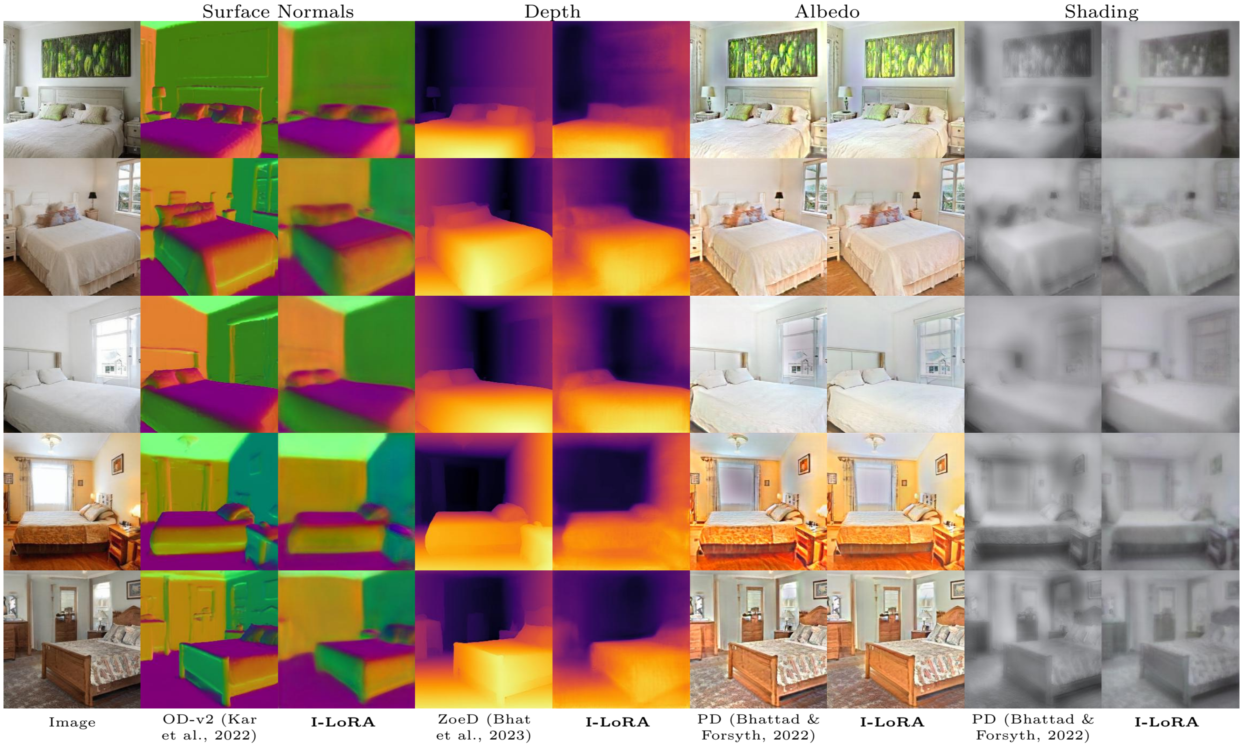

Figure 21: Additional results of scene intrinsics extraction from Stylegan-v2 trained on LSUN bedroom images.

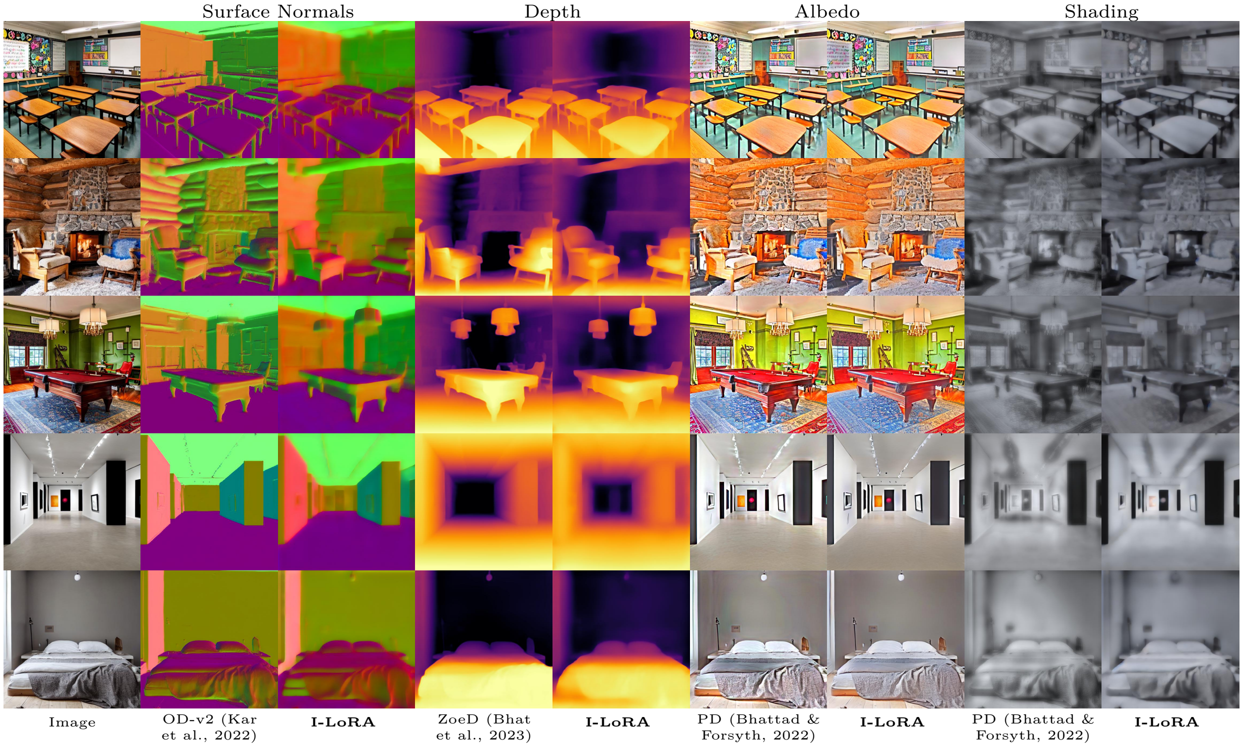

Figure 22: Additional results of scene intrinsics extraction from Stable Diffusion I-LoRA (single-step).

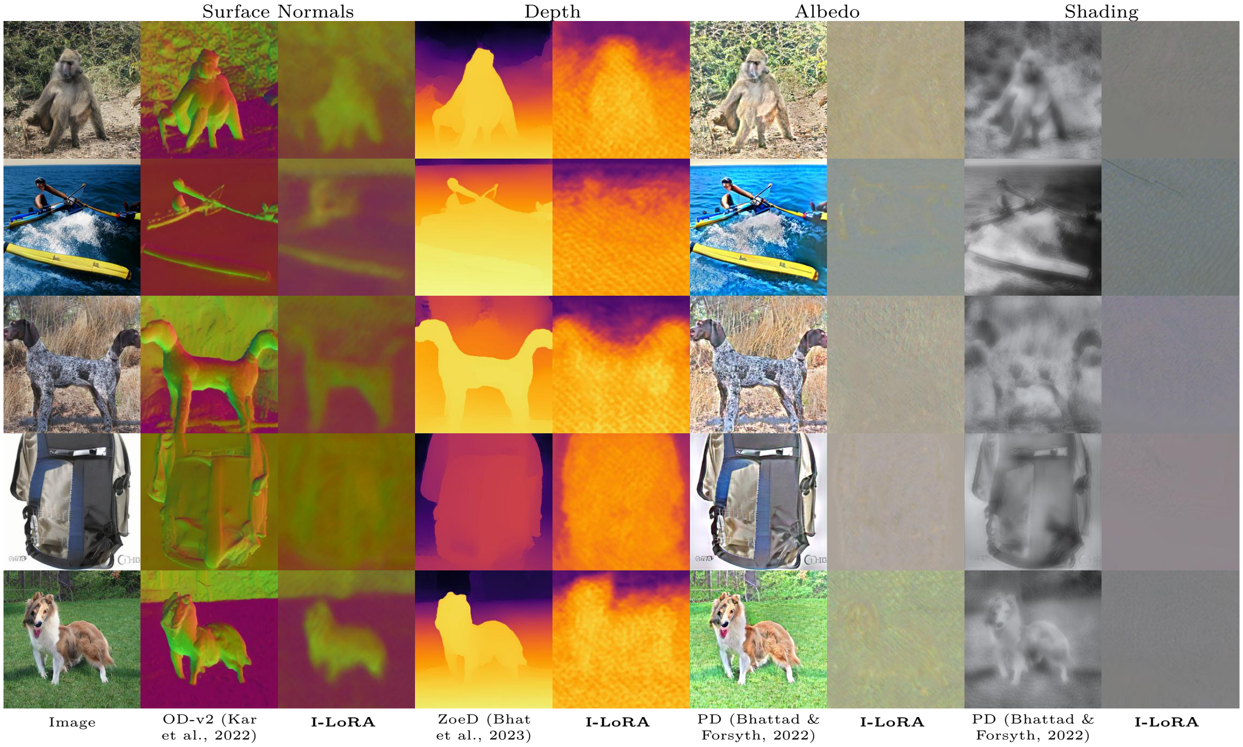

Figure 23: Additional results for StyleGAN-XL trained on ImageNet. StyleGAN-XL's inability to produce image intrinsics may be due to its inability to create high-quality plausible images.

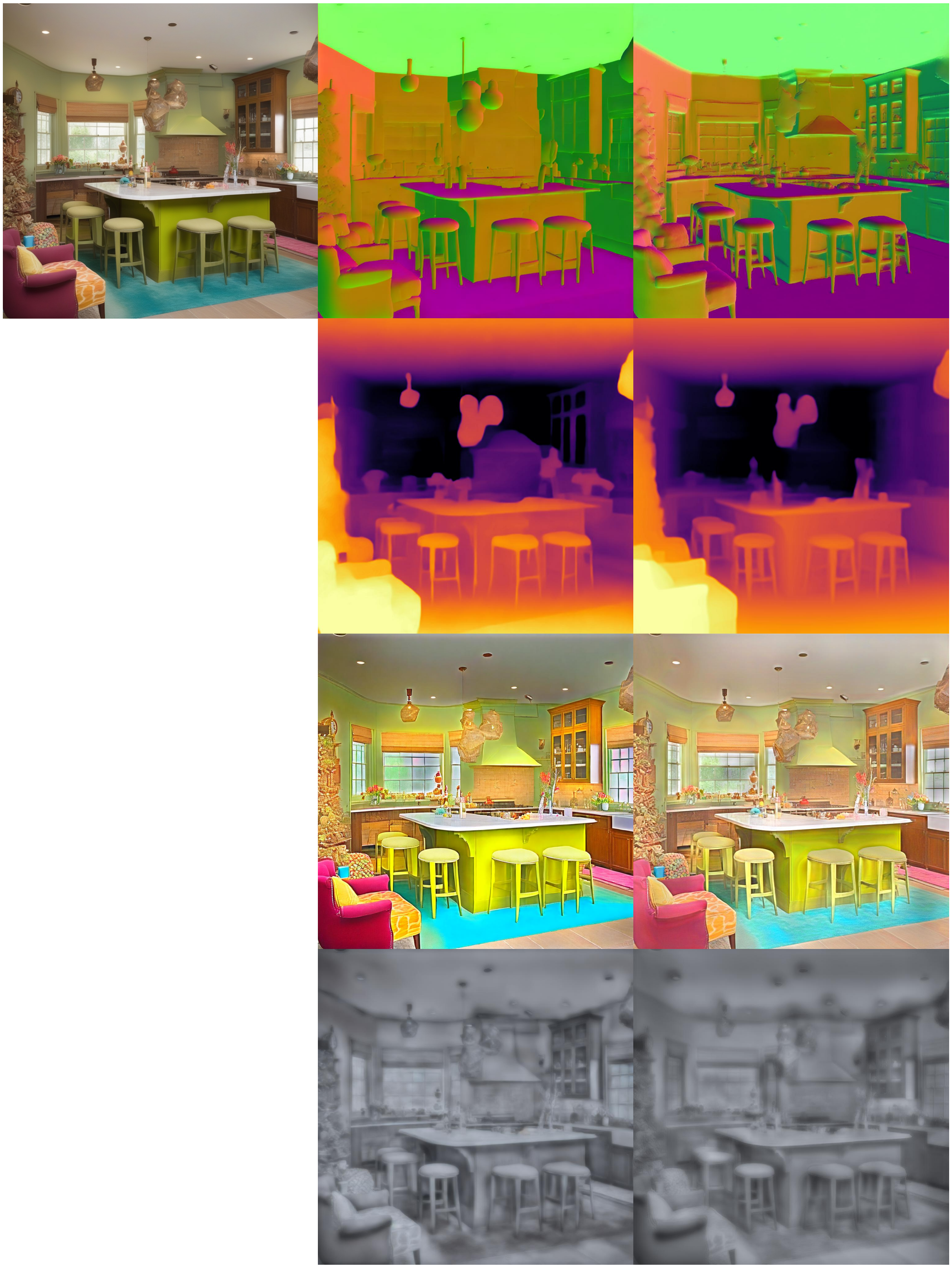

Figure 24: Results of I-LoRA$_{\text{AUG}}$ models applied on unseen 1024^2 synthetic images. Left: original image; middle: ours; right: pseudo ground truth.

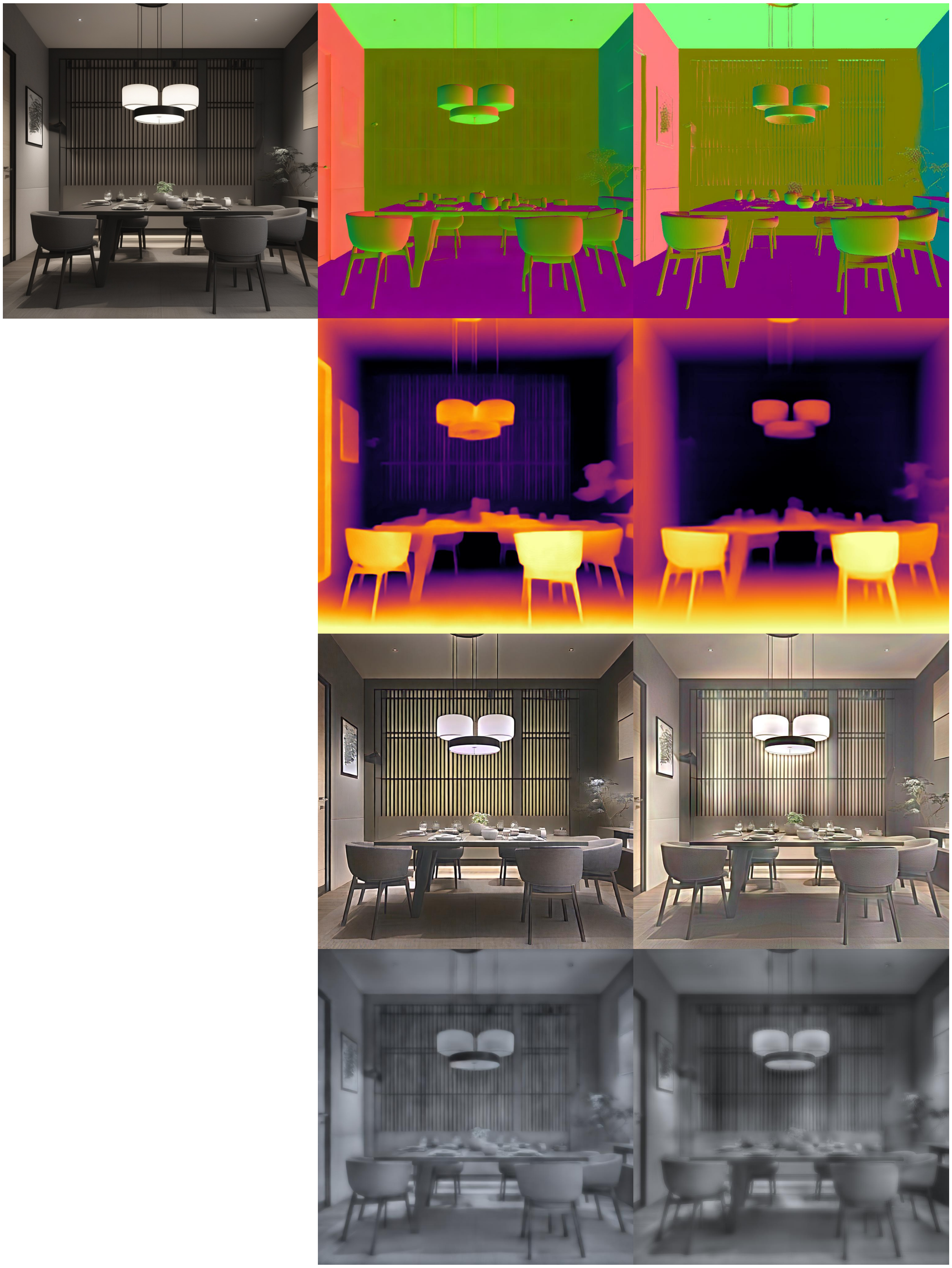

Figure 25: Cont. results of I-LoRA$_{\text{AUG}}$ models applied on unseen 1024^2 synthetic images. Left: original image; middle: ours; right: pseudo ground truth.

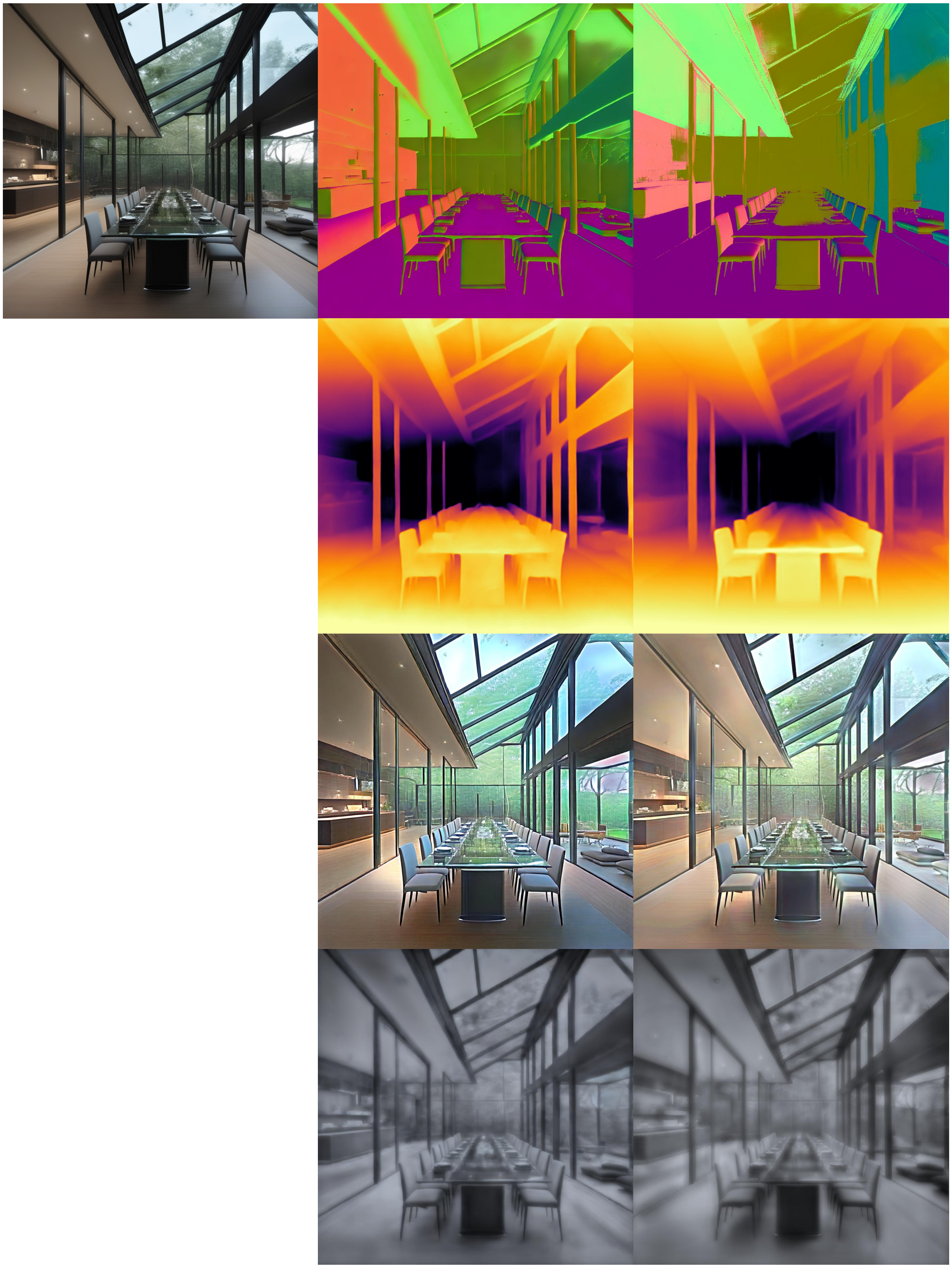

Figure 26: Cont. results of I-LoRA$_{\text{AUG}}$ models applied on unseen 1024^2 synthetic images. Left: original image; middle: ours; right: pseudo ground truth.

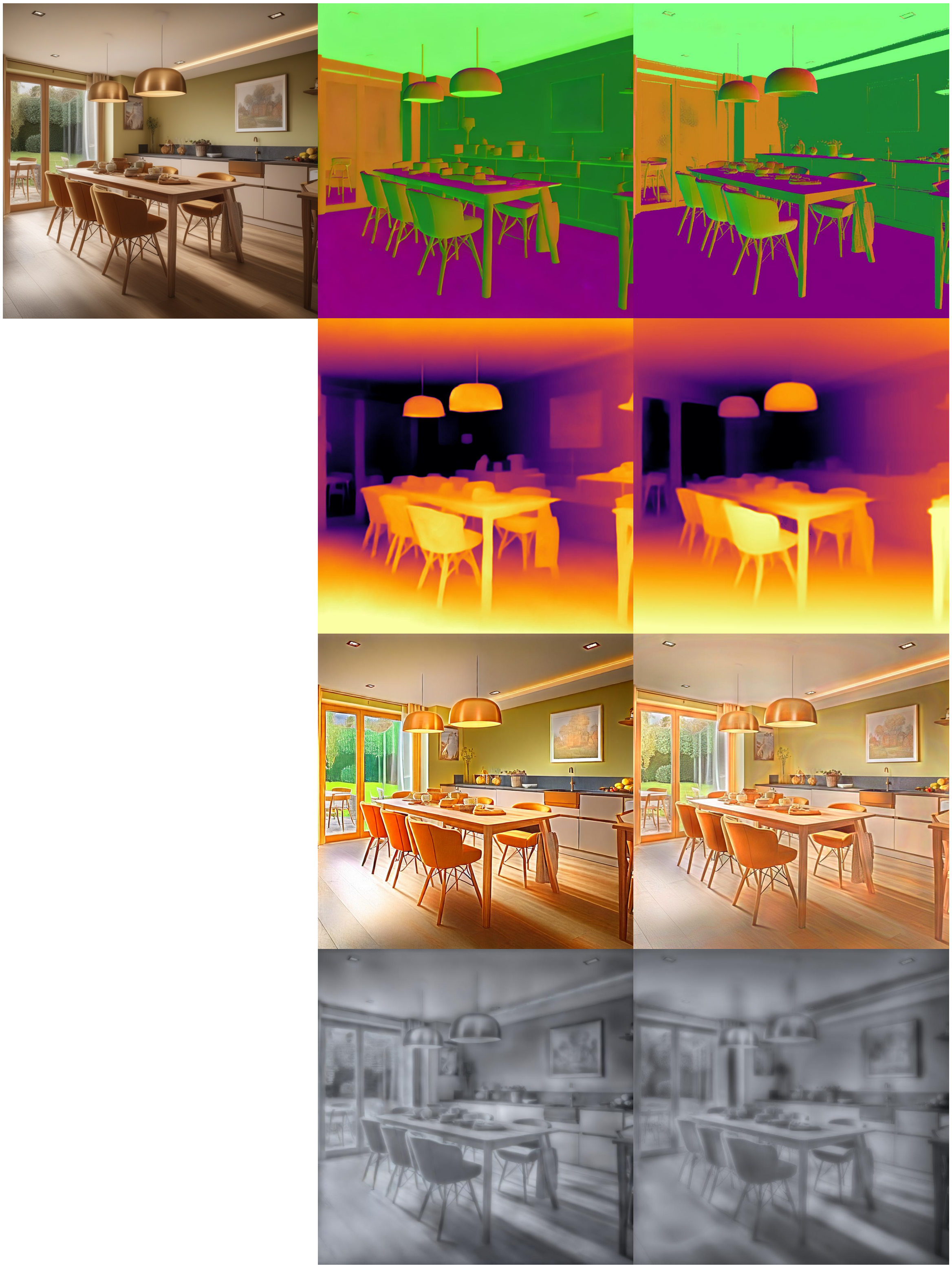

Figure 27: Cont. results of I-LoRA$_{\text{AUG}}$ models applied on unseen 1024^2 synthetic images. Left: original image; middle: ours; right: pseudo ground truth.

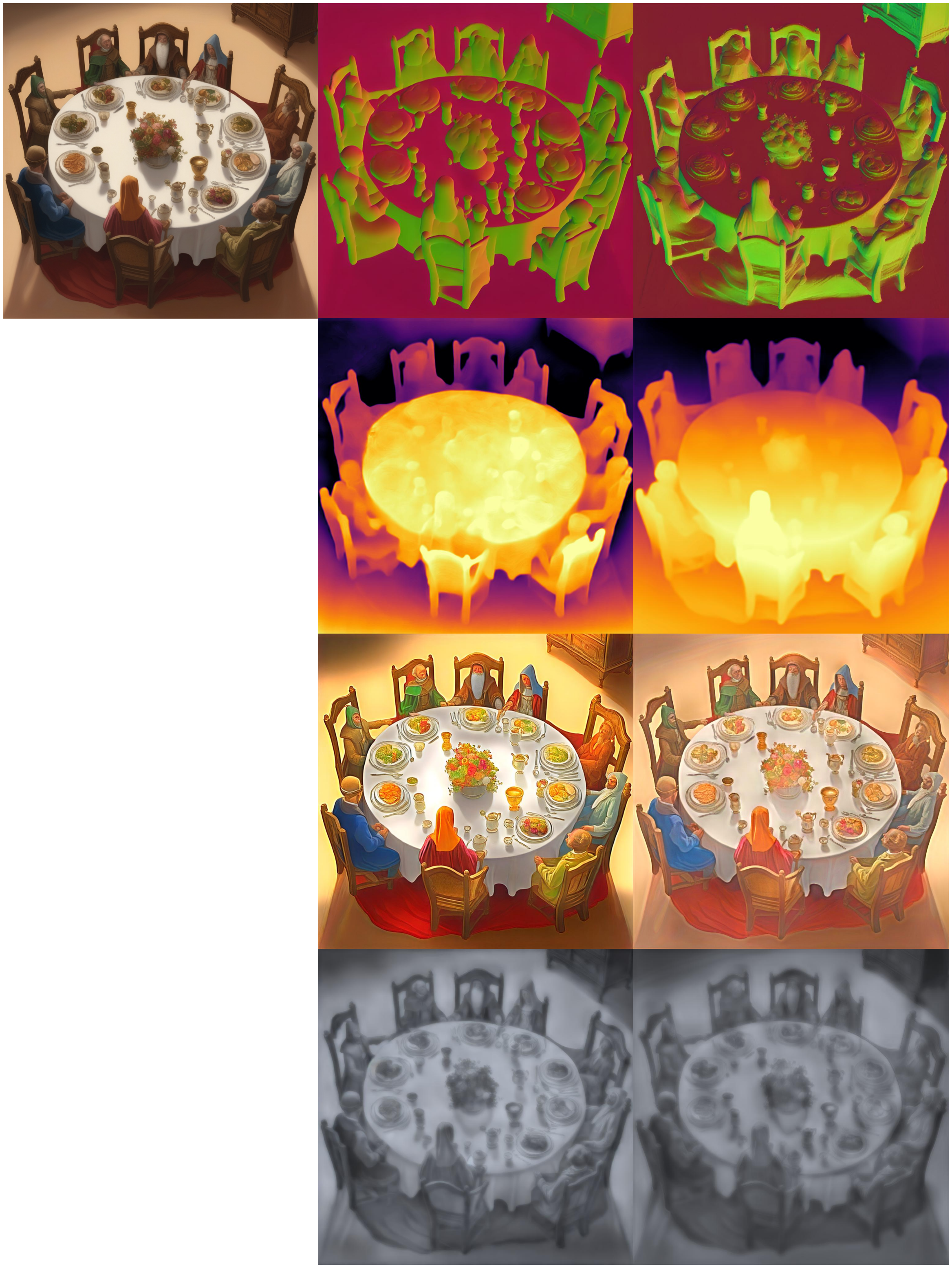

Figure 28: Cont. results of I-LoRA$_{\text{AUG}}$ models applied on unseen 1024^2 synthetic images. Left: original image; middle: ours; right: pseudo ground truth.

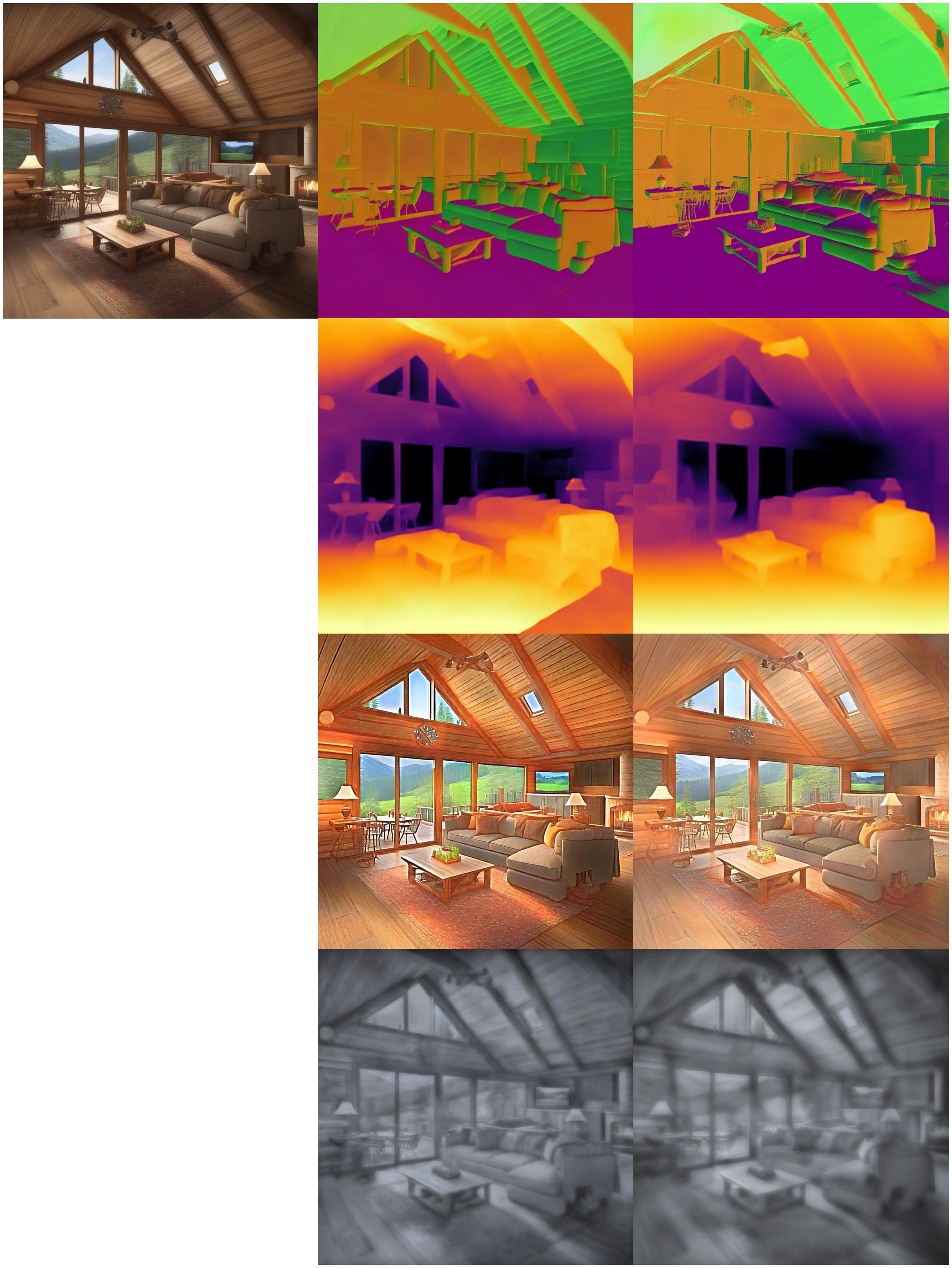

Figure 29: Cont. results of I-LoRA$_{\text{AUG}}$ models applied on unseen 1024^2 synthetic images. Left: original image; middle: ours; right: pseudo ground truth.

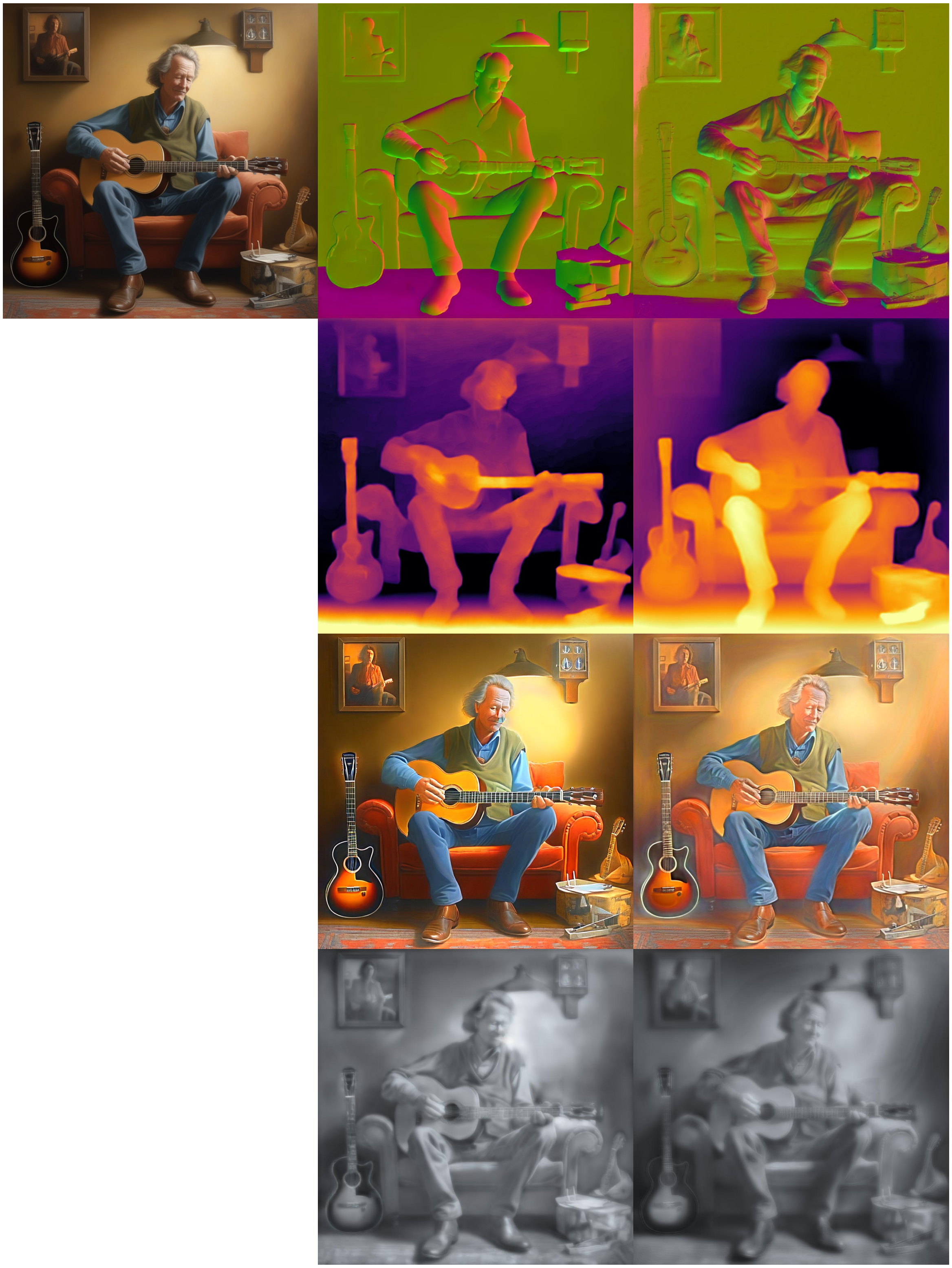

Figure 30: Cont. results of I-LoRA$_{\text{AUG}}$ models applied on unseen 1024^2 synthetic images. Left: original image; middle: ours; right: pseudo ground truth.

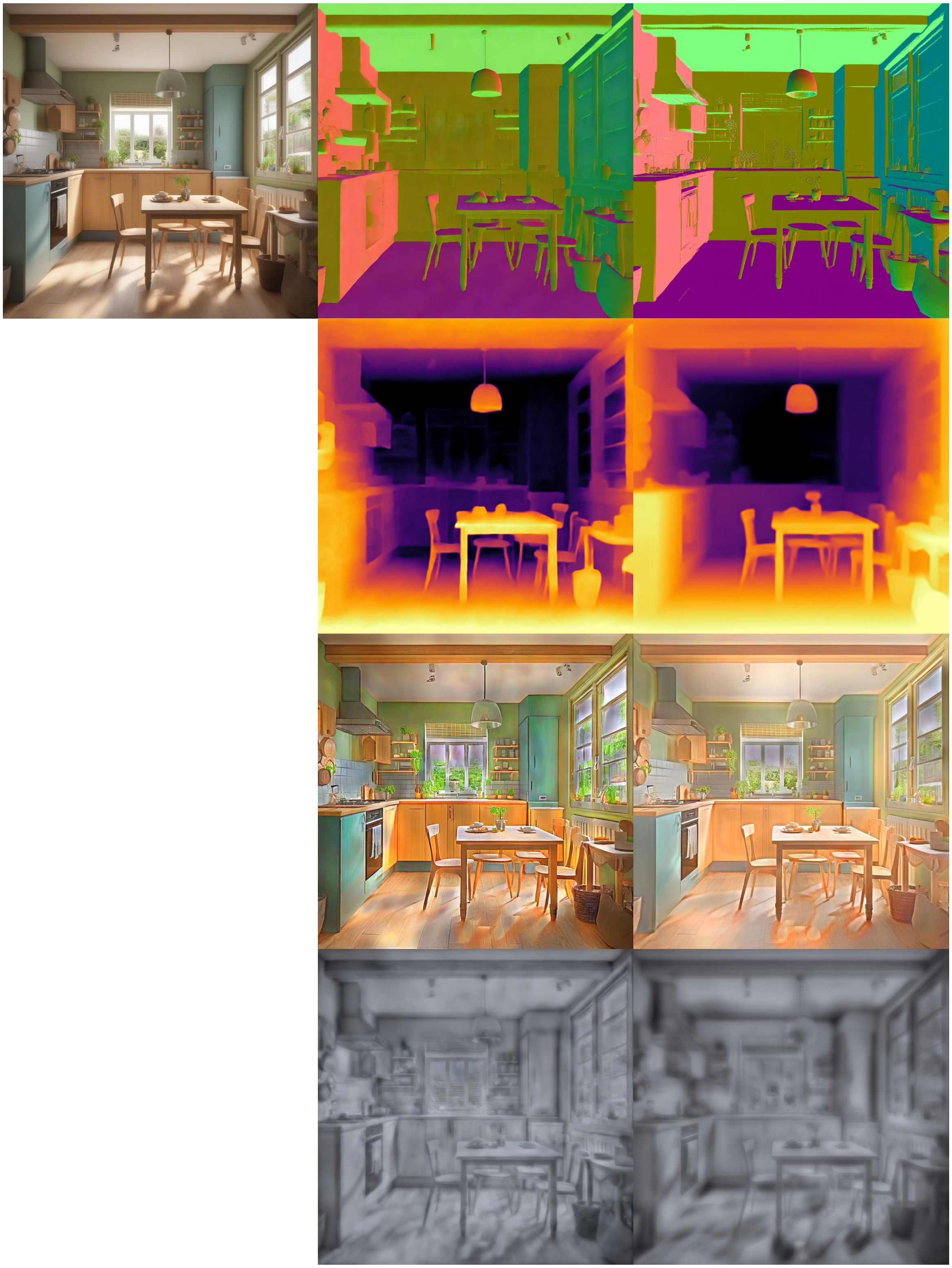

Figure 31: Cont. results of I-LoRA$_{\text{AUG}}$ models applied on unseen 1024^2 synthetic images. Left: original image; middle: ours; right: pseudo ground truth.

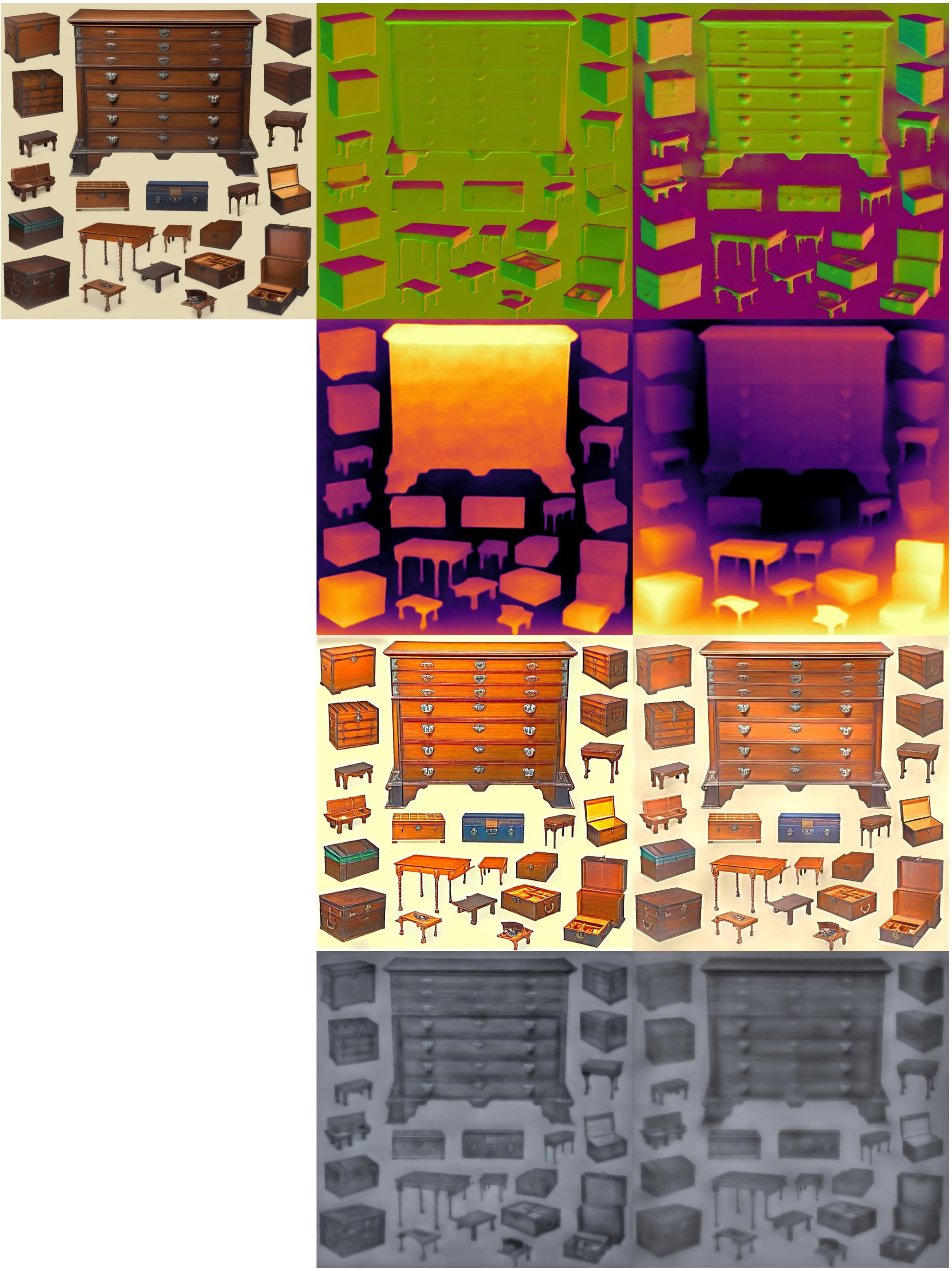

Figure 32: Cont. results of I-LoRA$_{\text{AUG}}$ models applied on unseen 1024^2 synthetic images. Left: original image; middle: ours; right: pseudo ground truth.

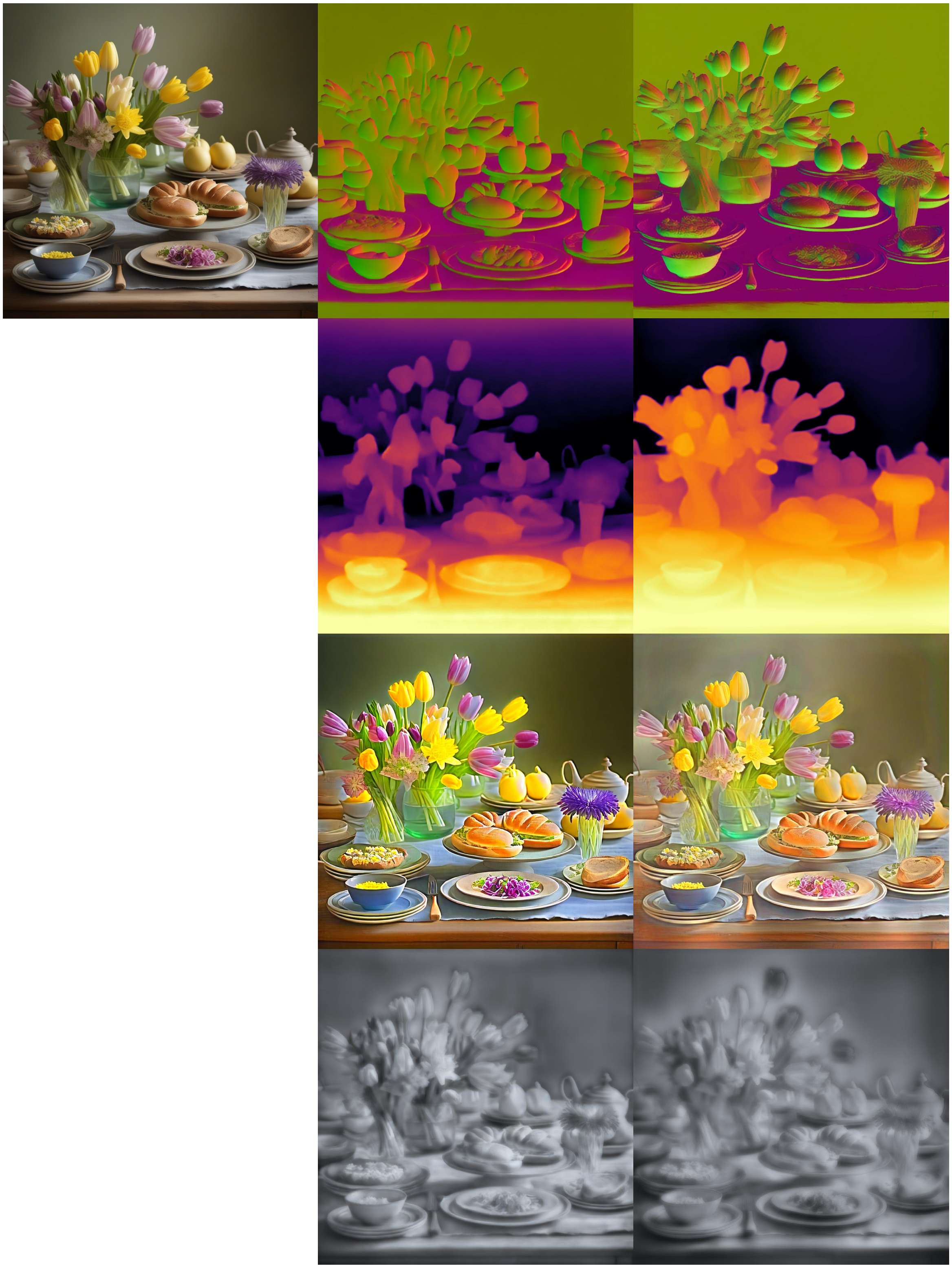

Figure 33: Cont. results of I-LoRA$_{\text{AUG}}$ models applied on unseen 1024^2 synthetic images. Left: original image; middle: ours; right: pseudo ground truth.